Tox reinforces the phenotype and longevity of dysfunctional T cell populations during chronic viral infection

Francesca Alfei[1], Kristiyan Kanev[1], Maike Hofmann[2], Ming Wu[1], Hazem E. Ghoneim[4], Patrick Roelli[1,3], Daniel T. Utzschneider[5], Madlaina von Hösslin[1], Jolie Cullen[1], Yiping Fan[6], Vasyl Eisenberg[7], Dirk Wohlleber[8], Katja Steiger[9], Doron Merkler[10], Mauro Delorenzi[3], Percy A. Knolle[4], Cyrille J. Cohen[7], Robert Thimme[2]*, Benjamin Youngblood[4]*, and Dietmar Zehn[1]*

[1] Division of Animal Physiology and Immunology, School of Life Sciences Weihenstephan, Technical University of Munich, 85354 Freising, Germany

[2] Universitätsklinikum Freiburg, Klinik für Innere Medizin II, University of Freiburg, 79106 Freiburg, Germany

[3]SIB, Swiss Institute of Bioinformatics, University of Lausanne 1015 Lausanne, Switzerland and Department of Oncology, University of Lausanne, 1011 Lausanne, Switzerland

[4] Department of Immunology, St. Jude Children's Research Hospital, Memphis, TN 38105-3678, United States

[5] Department of Microbiology and Immunology, The University of Melbourne and The Peter Doherty Institute for Infection and Immunity, Melbourne, VIC 3000, Australia

[6] The Department of Computational Biology, St. Jude Children's Research Hospital, Memphis, TN 38105, USA

[7] The Mina and Everard Goodman Faculty of Life Sciences, Bar-Ilan University, Ramat Gan 5290002, Israel

[8] Institute of Molecular Immunology and Experimental Oncology, University Hospital Klinikum rechts der Isar, Technical University of Munich, 81675 Germany

[9] Comparative Experimental Pathology, Institute of Pathology, Technical University of Munich, 81675 Munich, Germany

[10] Department of Pathology and Immunology, University of Geneva, 1211 Geneva, Switzerland

***Corresponding authors:**

Dietmar Zehn, Division of Animal Physiology and Immunology, School of Life Sciences Weihenstephan, Technical University of Munich, 85354 Freising, Germany, Phone: +49 (8161) 71 3508, Email: dietmar.zehn@tum.de

Benjamin Youngblood, The Department of Immunology, St. Jude Children's Research Hospital, Memphis, TN 38105, USA, Phone : +1 901 595 2332, Email: Benjamin.youngblood@stjude.org

Robert Thimme, Universitätsklinikum Freiburg, Klinik für Innere Medizin II, University of Freiburg, 79106 Freiburg, Germany, Phone: +49 (761) 270-34040, Email: robert.thimme@uniklinik-freiburg.de

Abstract:

Chronic CD8 T-cell stimulation in persisting infections or tumors can induce a stable gene expression program, known as T-cell dysfunction or exhaustion, that limits the cell's effector functions and anti-viral and anti-tumor immunity. Thus far, the underlaying molecular mechanisms that induce and stabilize this phenotype are vaguely understood. We report here that establishing this program requires the thymocyte selection-associated high mobility group-box protein (Tox). Genetic disruption of Tox augments effector function, decreases the expression of PD-1, and significantly enhances immunopathology. These changes are linked to a failure in fixing the dysfunctional phenotype in the critical Tcf1$^+$ progenitor population and to impaired epigenetic programing. Surprisingly, the gains in effector function co-incide with declining numbers of Tcf1$^+$ cells and result ultimately in reduced total numbers of pathogen-specific T-cells. Thus, we establish Tox as a critical factor for the development of T-cell dysfunction and establish a clear link between CD8 T-cell intrinsic suppression of effector function and protection against immune-pathology.

Main Text:

Prolonged exposure of T cells to their cognate antigen during chronic infections and cancer can result in suppression of the T cell's cytolytic functions, a reduction of their cytokine production capacity, and increased expression of inhibitory receptors such as PD-1[1-6]. Recent observations indicate that this process is associated with mechanisms that enforce cellular differentiation, specifically the acquisition of long-lived epigenetic modifications to the genome[7]. As a consequence, simply removing T cells from the source of antigen is not sufficient to restore their effector functions. Akin to these adoptive transfer studies, recent studies assessing the longevity of T cell responses during immune checkpoint blockade therapy have established that the T cells that respond to check-point inhibitors eventually revert back to their dysfunctional state, indicating that the cells had already undergone a differentiation program that committed them to the dysfunctional state[8-11]. Similar to the murine studies, hepatitis C virus-specific T cells in humans retain key features of their dysfunctional phenotype after pharmacological resolution of the infection[12]. Importantly, this 'dysfunctional' program is imprinted in the proliferation competent Tcf1^{+} progenitor population, which serves to maintain the T cell response during a chronic infection or cancer. Thus, this commitment is coupled to the stable propagation of the dysfunctional effector program upon proliferation of the progenitors.

To date, the mechanism(s) that enforce the dysfunctional program remain vaguely understood, however a key feature driving this commitment appears to be the quality of the TCR signal; T cell dysfunction is observed under conditions where antigen levels remain high for long periods of time[13]. Several transcription factors including Irf4, Nr4a1, or Nfatc1[14-16] are known to impact the differentiation of T cells during chronic infection, yet the same factors are also active during T cell responses to acute infections. How these factors individually or in an interactive

fashion can lead to such divergent phenotypic and functional outcomes and which molecular mechanisms downstream of the classical TCR signaling cascade sense the level of TCR stimulation and generate dysfunctional phenotype remain to be fully explored. Here we report a previously unrecognized role for the thymocyte selection-associated high mobility group box protein (Tox)[17, 18] in reinforcing the dysfunctional phenotype in mouse and human T cells.

The murine model of *Lymphocytic choriomeningitis virus* (LCMV) consists of viral strains that result in acute or chronic infections, but retain the same dominant T cell epitopes[19]. This allows for direct comparison of T cells responding to the same epitopes such as the gp33-41 (gp33) in acute LCMV Armstrong or chronic LCMV clone-13 infection. This comparison was used to establish the phenotypic features and gene-expression profiles of "exhausted" or "dysfunctional" T cells[20]. However, a significant fraction of DEG in these signatures likely result from comparing T cells in two dissimilar infections, as LCMV clone-13 and Armstrong differ significantly in the level of tissue damage, inflammation, and in T cell expansion kinetics. We therefore undertook a modified approach through which we thought to more specifically enrich for gene-expression signatures that are linked to the presence or absence of a dysfunctional phenotype. Here we used a variation of the LCMV model system that we have previously documented to better reveal a direct link between the exhaustion phenotype and TCR stimulation[13]. This variation retains a chronic inflammatory environment while establishing a significant reduction in antigen quantity by mixing a gp33 epitope-deficient mutant LCMV virus with wild-type clone-13 at an approximately 5:1 ratio. This "mixed infection" causes gp33-specific T cells to retain a polyfunctional phenotype while T cells responding to other epitopes still exhibit a dysfunctional phenotype. By comparing gp33-specific T cells from these mixed versus pure wildtype chronic LCMV infection, we therefore obtained a set of differentially expressed genes [DEG], which more specifically reflects the molecular signature of dysfunctional versus normal polyfunctional T cells (**Supp.Fig. 1A**). Indeed, both cell populations expand in this setup with similar kinetics and are obtained from a similarly inflamed environment. The resulting DEG list with Log2FC $\geq |2|$ contains genes such as Tigit, Rgs16, Lag3, Klrg1, and Nr4a2, which were previously linked to T cell responses during chronic infection[16,21], but also new genes whose

significance remains unclear at present. To refine the association of these unknown genes with a dysfunctional phenotype, we obtained a second independent DEG list from another alternative approach that also establishes T cells with or without a dysfunctional phenotype obtained from the same environment. In this setup, we compared T cells from acute and chronic infection that were isolated from their respective infections, transferred into new hosts, and re-expanded by infecting the new hosts with LCMV Armstrong. As we have reported previously, both donor cells re-expanded following the Armstrong infection but the donor cells from the clone-13 infection retained core features of dysfunctional T cells[10] (**Supp.Fig. 1B)**. Thus, this second set of DEG reflect gene expression programs that become reinforced during chronic stimulation and which are retained when cells are removed from the source of antigen and inflammation. By examining the shared gene expression signatures among these two model systems, we reasoned that we would specifically enrich for DEGs that are critical for the dysfunctional phenotype. With a low threshold (Log2FC of $\geq|0,5|$) we find a 529 DEG overlap between both datasets but remarkably, there is 98% directional synergy (**Supp. Fig. 1C**). This means that almost all the overlapping DEG that are linked to T cell dysfunction or that are anti-correlated with T cell dysfunction are also linked or anti-correlated in the other dataset. As the measurements were done in different experimental setups, the very high directional synergy underscores the tight connection of the overlapping DEG with T cell dysfunction. Notably, a factor that scored very high on both lists was the high mobility box group transcription regulator Tox.

To explore the role of Tox in the development of T cell dysfunction, we proceeded to characterize Tox expression at protein level. Tox becomes detectable at the protein level in T cells at the early stage of a chronic, but not in acute LCMV infection. Its initial expression is antigen-dose but not affinity dependent (**Fig. 1A**). These results mirror reports that antigen amount and

the frequency of TCR triggering and not antigen-affinity determines T cell dysfunction[13]. Tox levels also increase transiently during positive selection in the thymus, which highlights a connection between Tox and TCR signaling beyond infections (**Supp.Fig. 2A, B**). To investigate if the chronic stimulation resulted in a reinforced change in the programming of Tox expression, P14 T cells were removed from the chronic infection and re-expanded during an acute infection (**Fig. 1A**). Indeed, only the P14 cells isolated from a chronic setting were able to express Tox under acute antigen settings. These data further confirm the pattern of Tox expression that we observed in the gene expression analysis (**Supp.Fig. 1B**). Thus, once established, T cells retain an ability to express Tox. Notably, this reinforcement of Tox expression correlated strongly with increasing de-methylations in the Tox promoter region that only occurred during chronic infection (**Fig. 1B**). Furthermore, P14 T cells that retain normal T cell function after chronic exposure to a low gp33 antigen quantity retained a partially methylated Tox promoter region. Thus, methylation pattern of the Tox promoter correlated with reinforcement of Tox expression and was coupled with development of T cell dysfunction.

Phenotypic analysis revealed that Tox correlates with PD-1 expression and that cells with the highest PD-1 expression within the total host $CD8^+$ T cell population showed also higher Tox expression (**Fig. 1C**). In contrast, Tox was absent in $KLRG1^+$ T cells (**Fig. 1D**). This is well in line with the fact that KLRG1 is prominently expressed on antigen-specific T cells in acutely resolved LCMV infection but not on exhausted cells in chronic LCMV infection.[21] These observations were verified in human chronic hepatitis C virus [HCV] infection, where augmented TOX expression coincided with PD-1 expression levels in HCV-specific T cells (**Fig. 1E**). Furthermore, TOX was detectable in T cells responding to chronic HCV infection, but was not detected in T cells generated in response to spontaneously resolved HCV infection. Additionally, we were unable to detect TOX expression

in influenza-specific human memory T cells, which are derived from acute infection. Interestingly, its expression was still detectable in individuals whose chronic HCV infection was successfully resolved using antiviral therapy, however TOX expression was slightly lower in this case (**Fig. 1E**). Thus, similar to the murine viral infection models, TOX expression in antigen-specific T cells is coupled to persisting viral infection in humans, and its expression becomes stably imprinted.

To further investigate the impact of Tox expression in the development of T cell exhaustion, we obtained from the international mouse knockout consortium a mouse allowing conditional deletion of the 5th exon of Tox [ToxΔ^{Ex5} mice]. Of note, the 5th exon covers the nuclear translocation sequence and ~2/3 of the DNA binding domain[22]. Thus, upon exon 5 deletion Tox may still serve as a signaling scaffold as the protein is still produced but its ability to translocate to the nucleus and its capacity to directly bind DNA should be eliminated according to current structural understanding of Tox[23]. This is different from other published conditional full Tox knockout mice from which the first exon can be eliminated[18,24]. The 5th exon was deleted by treating both Mx-CrexP14xRosa[stop]YFPxToxEx5$^{fl/fl}$ and control Mx-CrexP14xRosa[stop]YFP mice with polyIC 2-5 days prior to harvesting P14 T cells from these donors. After co-transfer, chimeric animals containing YFP^{+} wt and ToxΔ^{Ex5} YFP^{+} T cells were infected with the chronic strain of LCMV, and then the T cell response was measured. The comparable early PD-1 and CD69 expression among Wt and ToxΔ^{Ex5} T cells indicates that the cells had a comparable initial activation (**Supp. Fig. 3A, B**). However, at the peak of expansion or thereafter, ToxΔ^{Ex5} cells had reduced levels of PD-1 expression relative to wt T cells. Additionally, the ToxΔ^{Ex5} cells had retained a greater capacity for TNF and IFNγ production, and altered Tbet and Eomes ratios - all of which indicate retention of a more polyfunctional phenotype in the absence of Tox (**Fig. 2A-C**). Moreover, we noted increased KLRG-1 expression that prominently peaked on day 13 post infection (**Fig. 2E**).

This is striking as KLRG-1 expression is restricted to T cells in acutely resolved LCMV infection, while it is usually absent or expressed only at low level among antigen-specific T cells in chronic LCMV infection[21]. This observation further underlines that the ToxΔ^{Ex5} cells share features with cells generated during an acute infection. Similar phenotypic observations with wt and ToxΔ^{Ex5} P14 T cells were made with P14 T cells transferred into mice that harbor elevated clone-13 titers due to limited T cell receptor diversity (**Supp.Fig. 3C-E**). Of note, granzyme B expression is typically detected among dysfunctional T cells during LCMV clone-13 infection, and the expression of granzyme B was unchanged in the absence of Tox (**Supp.Fig. 3F**). Interestingly, the T cell phenotype remained unchanged when Exon 5 was eliminated from Tox beyond day 20 post infection, which suggests that Tox with Exon 5 is needed for the initial imprinting of the exhaustion phenotype, but is not needed for the immediate maintenance of a dysfunctional phenotype (**Supp.Fig. 4**). We detected a significant number of genes that were differentially expressed between ToxΔ^{Ex5} and wt P14s at day 8 post infection and even higher numbers on day 20 post infection (**Fig. 2E**). Genes depicted in the heatmap were derived from a very stringent threshold (Log2FC ≥|1|, adjusted p-value of ≤0.05, MeanExpression ≥50). Under these conditions, the day 8 DEG list included Helios (Ikzf-2), Bach2, Socs3 and ID-3. With a rather low threshold (Log2FC ≥|0.3|) we saw, as depicted in **Supp.Fig. 5A,** that 269 of these genes are also differentially expressed in the dataset shown in **Supp.Fig. 1A** (direct comparison of dysfunctional and normal T cells) and there is a 209 DEG overlap with the genes that become fixed in chronic clone 13 infection (dataset shown in **Supp.Fig. 1B**). Notably, the total overlap between the three datasets accounts still for 125 genes and includes molecules such as ID3, IKZF2, NR4A1, NR4A2, PDCD1 (encoding PD-1), and KLRG1 (**Supp.Fig. 5A**). Collectively, these results indicate that Tox modifies

the expression of a significant number of genes, and in particular, molecules for which critical connections to T cell dysfunction are established.

To better define the biological relationship among the genes impacted by Tox expression, we undertook an unbiased approach to identify Tox-associated transcriptional networks. Using 'Ingenuity pathway analysis' (Qiagen) based predictions, we assessed DEGs from normal and dysfunctional T cells (dataset from **Supp.Fig. 1A)** and from wt versus ToxΔ^{Ex5} T cells (dataset from **Fig. 2E)**. We used the upstream regulator analysis, which assigns a p-value to putative upstream regulator based on the representation of genes that are linked to this regulator in a given dataset. We surprisingly noted a ~60% overlap between the top regulators in both datasets (results not shown) and a striking correlation between the p-values that are assigned for both datasets (**Supp.Fig. 5B**). Of note, the top regulators defined by an arbitrary p-value threshold below 10^{-8} are linked to 152 of the 269 DEG overlap between both datasets. Moreover, a large fraction of the DEG from the Figure 2E dataset, which are linked to a top scoring regulator, are linked to the same regulator in the other dataset (**Supp.Fig. 5C**). This also underlines similar transcriptional activity pattern in both datasets. Ultimately, this shows that Tox is strongly linked to the transcriptional particularities in dysfunctional compared to normal T cells. Of the genes that were impacted by the absence of Tox in clone-13 infection, the vast majority are not differentially expressed in acute Armstrong infection (**Fig. 2E**). In addition, only a limited set of genes are impacted by the absence of Tox in acute infection (**Supp.Fig. 6E**). Moreover, we did not observe an altered tissue distribution pattern of wt and ToxΔ^{Ex5} P14s in the spleen (**Supp.Fig. 7A, B**). Altogether, the data indicate that Tox inhibits acute T cell differentiation, enforces a dysfunctional T cell phenotype, and acts specifically during chronic infection with little impact on T cell differentiation in acute infection.

To further investigate the requirement of Tox in establishing a dysfunctional phenotype, we retrovirally overexpressed human TOX in *ex-vivo* activated polyclonal T cells from healthy human donors. This resulted in a modest but detectable up-regulation of PD-1 expression. Following co-culture of the transduced cells with tumor cells, we observed lower amounts of IFNγ and TNF production. (**Supp.Fig. 8A, B**). Similar to our experiment with human T cells, we examined the impact of Tox overexpression on murine LCMV-specific T cells. Here we used the low antigen level chronic LCMV clone-13 model system which normally results in a retention of functional phenotype[13]. Yet, overexpression of Tox in this context induces phenotypic and functional properties of dysfunctional T cells including reduced KLRG-1 expression, lower TNF and IFNγ production, and increased PD-1 levels, while Tcf-1 MFI remained across all samples similar (**Supp.Fig. 8C-F**). Thus, knockout or overexpression of Tox in mouse and humans CD8 T cells supports the conclusion that Tox is a driver of the dysfunctional phenotype.

Next, we asked which upstream factors control or induce Tox expression. We focused our search on molecules linked to TCR signaling as our data indicate that strong TCR signals induce Tox and T cell dysfunction[13]. Following strong *ex vivo* TCR stimulation, we observed the expected upregulation of Nr4a1[25] but soon thereafter Tox expression selectively increased only in Nr4a1 positive T cells, whereas reducing the magnitude of TCR stimulation by lowering the concentration of the stimulating anti-CD3 antibody resulted in a fewer number of Nr4a1, and subsequently, Tox expressing T cells (**Supp.Fig. 9A**). In line with this, Nr4a1 and Tox were both exclusively up-regulated in normal clone-13 infection but not following lose dose gp33 clone-13 or Armstrong infection (**Supp.Fig. 9B**). Of note, *in vitro* overexpression of Nr4a1 increased Tox expression, which establishes a molecular link between the two transcription factors (**Supp.Fig. 9C**). Evidence for Nr4a1 binding to the Tox promotor along with other transcription factors, which

are linked to T cell dysfunction, was found in the Transcription Regulation Database (GTRD, *http://gtrd.biouml.org/*) (**Supp.Fig. 9D**) whereby Irf4 overexpression alone and at least under *in vitro* condition did not induce Tox. "Ingenuity pathway" database suggests 5 other putative up-stream regulators of Tox. However, we could not visualize any prominent singular activity when these regulators are connected with the list of DEG between normal and dysfunctional P14 T cells (**Supp.Fig. 9E**). In contrast, genes from the same list predict activation of Nr4a1 (**Supp.Fig. 9E**). Taking this analysis in the context of what is already known about Nr4a1 from published findings[15,26] and our own observations, then the data indicate that TCR signal strength regulates Nr4a1 expression which then translates into Tox expression prior to the development of the T cell exhaustion gene expression program.

To assess the effector capacity of ToxΔ^{Ex5} P14 T cells, we made again use of Vβ5 transgenic which have largely LCMV unresponsive T cell receptor repertoires. Without a P14 transfer, there is no significant endogenous CD8 T cell response to LCMV[10]. ToxΔ^{Ex5} P14s retained an acute phenotype also in these hosts (**Supp.Fig. 3**). Importantly, transfer of ToxΔ^{Ex5} P14s resulted in heightened viral control in the blood (**Fig. 2F**) and spleen of Vβ5 mice (**Fig. 2G**), as well as exaggerated weight loss (**Fig. 2H**) compared to mice that received wt P14 cells. These data suggest that ToxΔ^{Ex5} deficient T cells bear a higher potential to cause immunopathology. Compared to wt cells, ToxΔ^{Ex5} P14 T cells caused much more pronounced tissue damage and massive edemas in the lungs. Furthermore, the T cell infiltration shifted predominately from periportal localization to parenchymal infiltration, with notable formation of necrotic foci in the liver. Such pathology documents the heightened infection-associated organ damage that Tox expression serves to mitigate (**Supp.Fig. 10),** and broadly corroborates the prior results that absence of Tox increases T cell effector function.

Surprisingly, despite the improved initial viral control mediated by ToxΔ^{Ex5} P14s, virus titers still reached wt levels in the spleen as early as 14 days post infection. Interestingly, this eventual decline in viral control correlated with a reduction in the quantity of ToxΔ^{Ex5} P14 (both data not shown). This observation along with our gene expression data, which revealed higher expression of CD127, Sell, Bcl2, and CCR7 on day 8 post infection in wt T cells (**Fig. 2E**), suggests that ToxΔ^{Ex5} knockout T cells have a significant survival deficit. To investigate this possibility, we co-transferred wt and ToxΔ^{Ex5} P14s into mice challenged by either Armstrong, pure, or mixed clone-13 infections (**Fig. 3A**). Generally, the ToxΔ^{Ex5} P14s had a slight trend towards greater initial expansion than wt cells under all infection conditions (**Fig. 3B**). However, ToxΔ^{Ex5} cells were rapidly culled in clone-13 infections after days 7-10 (**Fig. 3B,C**). Not unexpectedly, this occurred even after low affinity stimulation (**Supp.Fig. 11A, B**) which, as shown in **Fig. 1A** still induces Tox (**Fig. 1A**). By contrast, ToxΔ^{Ex5} P14s were maintained in mixed clone-13 infection (**Fig. 3B, C**), a condition of low antigen exposure that does not induce T cell dysfunction. Similarly, ToxΔ^{Ex5} P14s formed normal numbers of memory T cells following resolution of acute LCMV Armstrong infection. Moreover, these memory T cells were able to undergo secondary expansion (**Supp.Fig. 6C, D)** and had largely unaltered gene expression profiles on day 8 post infection (**Supp.Fig. 6B**). Thus, T cell maintenance is only Tox-dependent during conditions that promote T cell dysfunction, but not when T cells acquire a polyfunctional phenotype.

Recent studies have demonstrated that T cell maintenance in acute and chronic infections is supported by a small subpopulation of stem-like Tcf1 expressing cells[27-29] , which we refer to as memory-like progenitor T cells. Focusing specifically on this subpopulation, we noted a decrease in the frequency of Tcf1^{+} in ToxΔ^{Ex5} P14 cells compared to the wt population on day 8 post infection (**Fig. 3D**). However, this was only because of the greater overall quantity of Tcf1^{-} ToxΔ^{Ex5}

P14 cells compared to Tcf1$^-$ wt P14 cells. In fact, the absolute quantity of wt and ToxΔ^{Ex5} Tcf1$^+$ P14 T cells were similar on day 8 post infection (**Fig. 3E**). In contrast, there was a ~80 fold-reduction in the quantity of ToxΔ^{Ex5} Tcf1$^+$ compared to wt Tcf1$^+$ P14 T cells on day 20 post infection suggesting that exon 5 results in a critical defect in the survival of Tcf1$^+$ cells ToxΔ^{Ex5} (**Fig. 3F**). Moreover, the quantity of Tcf1$^-$ ToxΔ^{Ex5} P14 T cells had also declined on day 20 with a similar magnitude relative to the wildtype population. Given that the Tcf1$^+$ cells serve as a precursor that can develop into the Tcf1$^-$ population[27], the impact of exon 5 deletion from Tox on the Tcf1$^+$ cell likely indirectly results in a reduction of Tcf1$^-$ cells. Notably, we saw similar proliferation among wt and ToxΔ^{Ex5} P14 populations at two weeks post infection (**Supp.Fig. 11C**). Thus, absence of Tox results primarily in a numerical reduction of the Tcf1$^+$ population without impacting their capacity to give rise to a Tcf1$^-$ progeny. Together, these results collectively suggest that there is a narrow window in the time frame for establishing T cell dysfunction in which modulation of Tox expression can have a long-term impact on the phenotype and major impact on T cell survival.

Interestingly, Tcf1$^+$ wt P14s, generated during a chronic LCMV infection in mice, co-expressed high levels of Tox and PD-1 (**Fig. 4A**). This expression was also observed among Tcf1$^+$ Tetramer$^+$ T cells in ongoing or cured HCV infection in humans (**Fig. 4B**). In contrast, PD-1 expression was significantly reduced in ToxΔ^{Ex5} T cells (**Fig. 4C**). As genetic ablation of PD-1 also impairs T cell maintenance in chronic infection[30], the reduction of PD-1 likely impairs survival or maintenance of the Tcf1$^+$ population. In fact, reduced PD-1 expression could lead to lower levels of inhibitory signals potentially driving the cells toward terminal differentiation. To better understand the role of Tox in regulating the differentiation and survival of the memory-like progenitor population, we broadly characterized gene expression profiles. To separate the Tcf1$^+$ progenitor subsets from Tcf1$^-$ cells without performing a nuclear stain for Tcf1, we used Tim3

expression as a surface surrogate marker to enrich for T cells with Tcf1 expression[31,32]. The read count difference in our NGS data between the wt Tim3$^+$ and Tim3$^-$ confirms this separation (**Fig. 2D**). Interestingly, the Tim3$^-$ population showed downregulation of molecules linked to central memory or naïve T cells such as Sell and Ccr7 but surprisingly upregulation of IL-2Ra. Pathway analysis revealed impaired survival programs and activated apoptotic pathways in ToxΔ^{Ex5} T cells (**Supp.Fig. 12**), which goes along with the loss of this population. Altogether, we conclude that Tox plays a dual and unexpected role in the survival of T cell during their chronic stimulation; by promoting the acquisition of the typical ('dysfunctional) phenotype in chronic infection, Tox actually facilitates long-term T cell maintenance during a chronic infection.

Most surprisingly, we noted a substantially higher number of DEG comparing WT and Tox KO in the Tim3$^+$ compared to the Tim3$^-$ population. In fact, genes such as CD25(Il2ra), Hobit (Zfp683), Blimp1 (Prdm1), and Helios (Ikzf2), which are critical for T cell activation, effector function, and T cell dysfunction are only differentially expressed in the Tim3$^-$ but not in the Tim3$^+$ subset (**Fig. 4D**). Of note, a similar number of Tcf1$^+$ T cells (**Fig. 3E, F**) were generated among the wt and ToxΔ^{Ex5} T cells, which indicates that the gene expression programming differences did at that stage not arise from selective survival of an improperly stimulated ToxΔ^{Ex5} subpopulation. Instead, our data indicate that the ToxΔ^{Ex5} linked failure to acquire a dysfunctional signature is a phenotypic trait that is initially for many molecules not apparent and in particular not at the population level, as the Tim3$^-$ (or Tcf1$^+$) populations accounts for only 10-20% of the total population of antigen-specific T cells. Yet, when the progeny of this population becomes more prevalent with time, then this trait of showing reduced signs of a dysfunctional phenotype is revealed and the overall phenotype of the population shifts towards a phenotype that resembles the differentiation of cells in an acute infection. This model would explain the increasing

differences in gene expression profiling of wt versus ToxΔ^{Ex5} between day 8 and day 20 post infection and the initially similar and then over-time increasing difference in PD-1 or KLRG-1 expression as shown in **Fig. 2A** and **2D**. Vice versa, this indicates from the perspective of the wild-type condition that Tox exerts a profound phenotypic programming impact on the progenitor population and that the Tox enforced stable dysfunctional effector program subsequently spreads from the Tcf1^{+} progenitors over to the entire population.

We next sought to gain further insight into the mechanisms that initiate and preserve the T cell dysfunction program. Our observation that T cells did not immediately change their phenotype following conditional deletion of the 5th exon after day 20 post infection suggested that Tox is only transiently required for inducing the dysfunctional phenotype and not needed for the phenotypic stability of terminally differentiated, Tcf1^{-} cells. The autonomous and heritable nature of these gene expression programs prompted us to investigate whether the Tox-associated programming was coupled to epigenetic remodeling of the T cells. To broadly identify epigenetic programs associated with Tox expression we performed whole-genome DNA methylation profiling at the early infection stage, but given our prior findings we segregated cells into the Tim3^{+} and Tim3^{-} subsets from WT and ToxΔ^{Ex5} T cells at the effector stage of the immune response. Broadly, this analysis revealed a striking impact in the genome wide changes in DNA methylation status that occur in T cells at this stage of the immune response among both subsets in the absence of Tox (**Supp.Fig. 13A, B**).

Further characterization of the epigenetic programs impacted by exon 5 deletion from Tox revealed that these were predominantly regions that underwent demethylation during the naïve to effector stage of the immune response. Indeed, among the differentially methylated regions between day 8 WT and ToxΔ^{Ex5} T cells, ~90% of these regions were demethylated in the WT T cells

relative to the ToxΔ^{Ex5} T cells and. Importantly, loci that were differentially methylated between ToxΔ^{Ex5} T cells and wild-type T cells matched DNA methylation patterns observed in naïve T cells. The enrichment for naïve-associated DNA methylation programs was most apparent in the ToxΔ^{Ex5} Tim3^{+} subset of cells, with 85% of the WT vs Tox DMRs overlapping with naïve vs WT DMRs. A similar enrichment of naïve-associated DNA methylation programs was also detected in the ToxΔ^{Ex5} Tim3^{-} subset of T cells, albeit with slightly less overlap (42% overlap with the naïve vs Tim3^{-} T cell differentially methylated regions, **Supp.Fig. 13C**). Ontology analyses of the genes-associated with the Tox-mediated epigenetic programming document a significant enrichment in epigenetic programs that are coupled to the Interferon gamma pathway, T cell homing, and NFAT signaling (**Supp.Fig. 13C, D**).

To further assess the impact of Tox on epigenetic programming we performed ATACseq analysis of chromatin accessibility among WT and ToxΔ^{Ex5} T cells at day 8 and 13 post chronic infection. Similar to our DNA methylation analyses, we observed a large number of differentially open chromatin regions between ToxΔ^{Ex5} and wild-type T cells, indicating that Tox has a profound impact on the genome-wide chromatin remodeling that occurs at this stage of the T cell response. Interestingly, we also noted time-dependent changes between wt and ToxΔ^{Ex5} T cells in chromatin accessibility profiles in the PD-1 and TNF locus occurring along with major global accessibility changes between day 8 and 13 (**Supp.Fig. 14 A, B**). Ontology analysis of the Tox-associated changes in chromatin accessibility among the total pool of T cells further confirmed that Tox-regulated changes in chromatin remodeling occurs at genes directly associated with T cell activation (**Supp.Fig. 14C, D**). Notably, these comprehensive changes in epigenetic programming (DNA methylation and chromatin accessibility) appear to precede the gross changes in gene expression and phenotype that manifest at a later time-point. Broadly, these data support a

model for the establishment and reinforcement of T cell exhaustion gene expression programs whereby Tox regulates the primary epigenetic remodeling of T cells, which in turn enables a Tox-independent mechanism for preserving the T cell exhaustion program throughout the chronic stage of the immune response.

To illustrate the impact of ToxΔ^{Ex5} on gene expression networks, we filtered the regulators we have identified in the analysis shown in **Supp.Fig. 5** for transcription factors or transcription regulators and plotted their p-values against the number of linked DEG (**Supp. Fig. 15B**). Highly scoring factor include Id3, Id2, and Nfatc2. The connections of these and other relevant regulators to the DEG list for day 8 wt and ToxΔ^{Ex5} T cells are shown in **Supp.Fig. 15C**. We then focused on the predicted ~Top30 regulators and overlaid differential expression profiles from wt versus ToxΔ^{Ex5} in day 8 Tim3^{+} and Tim3^{-} populations. This again revealed selective expression differences mainly in the Tim3^{-} but not in the Tim3^{+} datasets (**Supp.Fig. 15D**). Moreover, it suggests that Tox induced alteration in effector programming involves strong activity changes in ID2, ID3, FoxM1, Bach2 networks along with Nr4a1, which we consider to be located upstream of Tox.

Our data demonstrate that Tox is a critical regulator for enforcing the transcriptional profile of dysfunctional T cells, while the acute phenotype appears to be the default differentiation pathway T cells acquire in the absence of Tox. Acquisition of a dysfunctional phenotype therefore reflects a well-regulated functional adaptation of T cells to the conditions of chronic infection. Moreover, our data show that this phenotype protects T cells and preserves the proliferative potential of the critical Tcf1^{+} memory-like progenitor population. These beneficial aspects contrast with the view that an “exhausted” phenotype signals that T cell populations have reached a terminal differentiation stage. Instead, the dysfunctional phenotype has likely evolved to protect the host in situations of failed pathogen elimination[2] and against overwhelming

pathology that is seen upon Tox elimination. Accordingly, the attenuation of T cell effector function possibly results in an equilibrium between the degree of T cell mediated virus control and the level of tissue pathology caused by the immune-response or the pathogen[20,33,34].

Notably, the phenotypic changes resulting from exon 5 deleted Tox are predominantly observed in the Tcf1^{+}/Tim3^{-} memory-like progenitor population at the early stage of the immune response, however, the impact of the deletion is increasingly observed among the total pool of antigen-specific T cells over time. Based on our collective data, we propose the dynamic model illustrated in **Supp.Fig. 16** to explain the over-time accumulating phenotypic changes and which highlights the role of Tox in the stable commitment of T cells to a dysfunctional state during chronic antigen exposure. Overall, we conclude that CD8 T cell dysfunction represents a particular form of epigenetically enforced effector differentiation, for which Tox is a highly critical, differentiation type deciding molecule. This discovery provides new potential therapeutic opportunities that involve manipulation of Tox expression to provide a transient T cell responses of strong magnitude and with high effector capacity.

Acknowledgements:

We would like to thank Mike J. Bevan for his input his feedback and suggestions and Tobias Herbinger, Brigitte Dötterböck, and Waltraud Schmid for technical assistance and animal husbandry. The work of the D. Z. lab was supported by the European Research Council starting and consolidator grants (ProtecTC, and ToCCaTa), grants from the Swiss National Science Foundation (CRSII3_160708, 310030E-164187, 51PHP0_157319, PP00P3_144883), the Swiss Vaccine Research Institute (SVRI) and from the German Research Foundation (SFB1054). DZ and CJC are supported by German-Israeli Foundation for Scientific Research and Development (GIF) Grant (No. I-1440-414.13/2017). KS is supported by the German Research Foundation grants (SFB824, SFB1335). RT and MH (Maike Hofmann) are funded by a German Research Foundation grant TRR179-TP01. BY is supported by the NIH (R01AI114442) and the American Lebanese Syrian Associated Charities (ALSAC). PK is supported by the Germany Center for Infection Research Munich site and the CRC TRR179.

Declarations:

We declare that there is no conflict of interest linked to the presented manuscript and the work that has been performed.

All experiments involving animal work and the use of regulated biological substances were approved by the responsible authorities in Switzerland and Germany.

Figure legends

Figure 1 - Dysfunctional T cells in mice and human express the transcriptional regulator Tox. **A**, Tox expression in P14 TCR-transgenic CD8 T cells isolated from C57BL/6 hosts at day 7 (upper row) or day 28 (middle row) post infection with $2x10^5$ PFU LCMV Armstrong, $5x10^6$ PFU wild-type or mutant clone-13 expressing a low affinity altered peptide ligand [13], or $5x10^5$ wild-type mixed with $4.5x10^6$ PFU mutant clone-13 that lacks the gp33 epitope (low epitope amount, mixed mutant infection). Lower row: Tox expression in P14 T cells that resided for 28 days in either LCMV Armstrong or clone-13 infected mice and were then transferred into new hosts and expanded for 8 days in acute LCMV Armstrong infection. Grey shadows are endogenous CD8 and colored lines P14 T cells. **B**, Top**,** a snapshot of whole-genome bisulfite DNA-methylation analysis in the Tox locus among naïve, LCMV Armstrong expanded $KLRG1^{high}CD127^{low}$ (TE), $KLRG1^{low}CD127^{high}$ (MP), and day 30 memory P14 T cells versus LCMV clone-13 primed day 8 (early) or 35 (late) P14 cells. Vertical lines indicate CpG positions and the red to black ratio the percentage of unmethylated versus CpG sequencing methylated reads. Bottom, loci-specific bisulfite sequencing analysis of the Tox locus in P14 CD8 T cells isolated 8 weeks post LCMV infection using Mixed, Armstrong, or pure clone 13 strains. Horizontal lines represent individual sequenced clones. Filled circles, methylated cytosine; open circles, nonmethylated cytosine. Bar graphs for CpG methylation are derived from 3 or more independent experiments. **C**, day 8 KLRG1 and Tox expression in Armstrong and clone-13 infections. **D**, day 8 PD-1 and Tox expression in total endogenous or P14 T cells in clone-13 infected hosts. **E**, TOX and PD-1 expression among virus specific ($Tetramer^+$) T cells in ongoing, treated, spontaneously resolved Human Hepatitis C infections, and among influenza-specific ($Tetramer^+$) memory T cells. Shown are representative dot plots and histograms

for selected donors and TOX and PD1 MFI for multiple donors. The lower Graph shows the correlation of TOX and PD-1 expression in the corresponding infections. Patient related data are included in the methods section. Mouse data are representative of three independently performed experiments, with at least 4 mice per group. Symbols represent individual mice, with the mean shown. Unpaired t-test were performed with *<0.05; **p < 0.01; ns = not significant (p > 0.05).

Figure 2 - Tox expression induces a dysfunctional phenotype and restricts T cell effector function. **A-D**, C57BL/6 recipient mice received $2x10^3$ Yfp^+ wt or Yfp^+ exon 5 deficient (ΔTox) P14 T cells. Both were obtained by flow cytometry based cell sorting of T cells isolated from PolyIC treated Mx-Cre/RosaYfp/P14 or MX-Cre/RosaYFP/P14/LoxPTox donor mice. Recipients were infected with $5x10^6$ PFU LCMV clone-13 and in some cases with LCMV Armstrong. PD-1 levels (A), cytokine production following *in vitro* gp33 re-stimulation in the presence of Brefeldin A (B), Eomes and T-bet expression (C), and KLRG-1 expression (D) were analyzed on day 8, day 13, or 20 post infection as indicated on top (D). Shown are representative flow plots for selected time-points and data for the analyzed time-points in the adjacent graphs. **E**, wt or $\underline{\text{Tox}\Delta^{Ex5}}$ P14 T cells were analyzed for global gene-expression on days 8 (left) and 20 post infection (right). **Upper row**, unfiltered Volcano plots showing Log2FC of wt/$\underline{\text{Tox}\Delta^{Ex5}}$ plotted against negative Log10 of the adjusted p-value. Orange dots are genes upregulated in wt and green dots are up-regulated in ΔTox. Dotted lines are set to Log2FC of 1 and -1 and adj. p-value of 0.05. **Lower row plots**, genes were filtered for mean expression levels (base mean values from deseq2 package) ≥ 50 and adj. p-value ≤ 0.05 and Log2FC ≥ 1 or ≤ -1 and wt/$\underline{\text{Tox}\Delta^{Ex5}}$ Log2FC are plotted against mean expression values. Lines are set to mean expression values of 50, 200, 500, annotated are the number of

genes above the lines, gene of interest are highlighted in color and names are annotated. **Heatmaps represent a** supervised selection of molecules from the plots shown above and they illustrate differential gene expression z-scores determined by the dseq2 package as explained in the methods section. **F-J**, Vβ5 mice, which carry the TCR-beta chain of OT-1 T cells and whose T cells are impaired in responding to LCMV, were engrafted with 10^4 wt or ToxΔ^{Ex5} P14 T cells and infected with $5x10^6$ PFU LCMV clone-13. Mice were analyzed on day 7 for viral titers in the blood (**F**) and spleen, and for numbers of P14s in the spleen (**G**). Bodyweight decrease is shown for day 14 (**H**). With the exception of the gene expression measurements, data are representative for three independently performed experiments, with at least 4 mice per group. In H data from three independent experiments are jointly presented. Symbols represent individual mice, the mean is shown. Unpaired t-tests were performed with *$p<0.05$; **$p < 0.01$; ns = not significant ($p > 0.05$).

Figure 3 - Tox is required for the maintenance of dysfunctional but not of normal effector or memory T cell populations. A, Schematic illustration of experimental procedure. Similar as explained in figure 2, $2x10^3$ CD45.1/1 ToxΔ^{Ex5} and $2x10^3$ CD45.1/2 wt P14 T cell, both obtained from PolyIC treated donor mice, were co-transferred in C57BL/6 recipients and infected with $2x10^5$ PFU LCMV Armstrong, $5x10^6$ PFU LCMV wt clone13, or $4{,}5x10^6$ PFU wt clone-13 wt and $5x10^5$ PFU LCMV gp-33 deficient clone-13 (gp33 low). **B**, **C** representative dot plots of the frequency and (B), kinetics of wt and ToxΔ^{Ex5} T cells at the indicated time-points (C). **D** Tcf1 expression MFI in Tcf1$^+$ wt and ToxΔ^{Ex5} P14 T cells on day 8 post LCMV clone-13 infection. **E-F**, representative histograms of P14 (solid colored lines) and data graphs showing the frequency and total numbers of Tcf1$^+$ P14 T cells on day 8 (**E**) and 20 (**F**) post infection. Gray shaded reference curves are total endogenous CD8$^+$ T cells. Data are representative for three independently

performed experiments, with at least 4 mice per group. Symbols are data for individual mice; solid horizontal lines represent the mean. Unpaired t test were performed with *<0.05; **p < 0.01; ns = not significant (p > 0.05).

Figure 4 - Proliferating precursor cells are predominantly impacted by the absence of Tox expression. A, Representative co-expression of Tox and Tcf1 and Tox and PD-1 MFI levels on $Tcf1^+$ and $Tcf1^-$ P14 TCR transgenic T cell on day 8 clone-13 infection. **B**, Tox expression in Tcf1 high cells in human HCV and Influenza-specific T cells as explained in Fig. 1E. **C**, Dot plots show Tcf1 and PD-1 co-expression levels on day 8 post infection for wt or $Tox\Delta^{Ex5}$ P14 T cells (mice were setup as explained in Fig. 2). Histograms indicate representative PD-1 expression levels in $Tcf1^+$ wt and $Tcf1^+$ $Tox\Delta^{Ex5}$ P14 T cells and corresponding PD-1 MFI data graphs for all animals. **D and E**, similar as in C, splenic wt and $Tox\Delta^{Ex5}$ P14 T cells were on day 8 sorted into $Tim3^+$ and $Tim3^-$ T cells and analyzed for global gene expression profiles. Tcf7 readcount differences between $Tim3^-$ and $Tim3^+$ are shown in D, **Upper row** (E) are unfiltered Volcano plots showing Log2FC of wt/$Tox\Delta^{Ex5}$ plotted against negative Log10 of the adjusted p-value. Orange dots are genes upregulated in wt and green dots are up-regulated in ΔTox. Dotted lines are set to Log2FC of 1 and -1 and adj. p-value of 0.05. **Lower row plots** (E) shows genes filtered for mean expression levels ≥ 50, Log2FC ≥ 1 or ≤ -1, and adj. p-value ≤0.05 and wt/$Tox\Delta^{Ex5}$ Log2FC are plotted against mean expression values. Lines are set to mean expression values of 50, 200, 500. Annotated are the number of genes above the lines. **Heatmaps represent a** supervised selection of molecules from the plots shown above and they illustrate differential gene expression z-scores determined by the dseq2 package as explained in the methods section. With the exception of the gene expression measurements, data are representative for at least two independently performed experiment, with at least 4 mice per

group. Symbols are data for individual mice, solid horizontal lines represent the mean. Unpaired t test were performed with *<0.05; **p < 0.01; ns = not significant (p > 0.05).

References

1 Wherry, E. J. T cell exhaustion. *Nat Immunol* **12**, 492-499 (2011).

2 Speiser, D. E. *et al.* T cell differentiation in chronic infection and cancer: functional adaptation or exhaustion? *Nat Rev Immunol* **14**, 768-774, doi:10.1038/nri3740 (2014).

3 Schietinger, A. & Greenberg, P. D. Tolerance and exhaustion: defining mechanisms of T cell dysfunction. *Trends Immunol* **35**, 51-60, doi:10.1016/j.it.2013.10.001 (2014).

4 Gallimore, A., Hengartner, H. & Zinkernagel, R. Hierarchies of antigen-specific cytotoxic T-cell responses. *Immunol Rev* **164**, 29-36 (1998).

5 Barber, D. L. *et al.* Restoring function in exhausted CD8 T cells during chronic viral infection. *Nature* **439**, 682-687, doi:10.1038/nature04444 (2006).

6 Chihara, N. *et al.* Induction and transcriptional regulation of the co-inhibitory gene module in T cells. *Nature* **558**, 454-459, doi:10.1038/s41586-018-0206-z (2018).

7 Youngblood, B. *et al.* Chronic virus infection enforces demethylation of the locus that encodes PD-1 in antigen-specific CD8(+) T cells. *Immunity* **35**, 400-412, doi:10.1016/j.immuni.2011.06.015 (2011).

8 Ghoneim, H. E. *et al.* De Novo Epigenetic Programs Inhibit PD-1 Blockade-Mediated T Cell Rejuvenation. *Cell* **170**, 142-157 e119, doi:10.1016/j.cell.2017.06.007 (2017).

9 Pauken, K. E. *et al.* Epigenetic stability of exhausted T cells limits durability of reinvigoration by PD-1 blockade. *Science* **354**, 1160-1165, doi:10.1126/science.aaf2807 (2016).

10 Utzschneider, D. T. *et al.* T cells maintain an exhausted phenotype after antigen withdrawal and population reexpansion. *Nat Immunol* **14**, 603-610, doi:10.1038/ni.2606 (2013).

11 Philip, M. *et al.* Chromatin states define tumour-specific T cell dysfunction and reprogramming. *Nature* **545**, 452-456, doi:10.1038/nature22367 (2017).

12 Wieland, D. *et al.* TCF1(+) hepatitis C virus-specific CD8(+) T cells are maintained after cessation of chronic antigen stimulation. *Nat Commun* **8**, 15050, doi:10.1038/ncomms15050 (2017).

13 Utzschneider, D. T. *et al.* High antigen levels induce an exhausted phenotype in a chronic infection without impairing T cell expansion and survival. *J Exp Med* **213**, 1819-1834, doi:10.1084/jem.20150598 (2016).

14 Man, K. *et al.* Transcription Factor IRF4 Promotes CD8(+) T Cell Exhaustion and Limits the Development of Memory-like T Cells during Chronic Infection. *Immunity* **47**, 1129-1141 e1125, doi:10.1016/j.immuni.2017.11.021 (2017).

15 Liu, X. *et al.* Genome-wide analysis identifies NR4A1 as a key mediator of T cell dysfunction. *Nature*, doi:10.1038/s41586-019-0979-8 (2019).

16 Martinez, G. J. *et al.* The transcription factor NFAT promotes exhaustion of activated CD8(+) T cells. *Immunity* **42**, 265-278, doi:10.1016/j.immuni.2015.01.006 (2015).

17 Aliahmad, P., Seksenyan, A. & Kaye, J. The many roles of TOX in the immune system. *Curr Opin Immunol* **24**, 173-177, doi:10.1016/j.coi.2011.12.001 (2012).

18 Page, N. *et al.* Expression of the DNA-Binding Factor TOX Promotes the Encephalitogenic Potential of Microbe-Induced Autoreactive CD8(+) T Cells. *Immunity* **48**, 937-950 e938, doi:10.1016/j.immuni.2018.04.005 (2018).

19 Virgin, H. W., Wherry, E. J. & Ahmed, R. Redefining chronic viral infection. *Cell* **138**, 30-50, doi:10.1016/j.cell.2009.06.036 (2009).
20 Doedens, A. L. *et al.* Hypoxia-inducible factors enhance the effector responses of CD8(+) T cells to persistent antigen. *Nat Immunol* **14**, 1173-1182, doi:10.1038/ni.2714 (2013).
21 Wherry, E. J. *et al.* Molecular signature of CD8+ T cell exhaustion during chronic viral infection. *Immunity* **27**, 670-684, doi:10.1016/j.immuni.2007.09.006 (2007).
22 O'Flaherty, E. & Kaye, J. TOX defines a conserved subfamily of HMG-box proteins. *BMC Genomics* **4**, 13 (2003).
23 Seehus, C. R. *et al.* The development of innate lymphoid cells requires TOX-dependent generation of a common innate lymphoid cell progenitor. *Nat Immunol* **16**, 599-608, doi:10.1038/ni.3168 (2015).
24 Aliahmad, P., de la Torre, B. & Kaye, J. Shared dependence on the DNA-binding factor TOX for the development of lymphoid tissue-inducer cell and NK cell lineages. *Nat Immunol* **11**, 945-952, doi:10.1038/ni.1930 (2010).
25 Moran, A. E. *et al.* T cell receptor signal strength in Treg and iNKT cell development demonstrated by a novel fluorescent reporter mouse. *J Exp Med* **208**, 1279-1289, doi:10.1084/jem.20110308 (2011).
26 Chen, J. *et al.* NR4A transcription factors limit CAR T cell function in solid tumours. *Nature*, doi:10.1038/s41586-019-0985-x (2019).
27 Utzschneider, D. T. *et al.* T Cell Factor 1-Expressing Memory-like CD8(+) T Cells Sustain the Immune Response to Chronic Viral Infections. *Immunity* **45**, 415-427, doi:10.1016/j.immuni.2016.07.021 (2016).
28 Lin, W. W. *et al.* CD8(+) T Lymphocyte Self-Renewal during Effector Cell Determination. *Cell Rep* **17**, 1773-1782, doi:10.1016/j.celrep.2016.10.032 (2016).
29 Yu, S. *et al.* The TCF-1 and LEF-1 transcription factors have cooperative and opposing roles in T cell development and malignancy. *Immunity* **37**, 813-826, doi:10.1016/j.immuni.2012.08.009 (2012).
30 Odorizzi, P. M., Pauken, K. E., Paley, M. A., Sharpe, A. & Wherry, E. J. Genetic absence of PD-1 promotes accumulation of terminally differentiated exhausted CD8+ T cells. *J Exp Med* **212**, 1125-1137, doi:10.1084/jem.20142237 (2015).
31 Delpoux, A., Lai, C. Y., Hedrick, S. M. & Doedens, A. L. FOXO1 opposition of CD8(+) T cell effector programming confers early memory properties and phenotypic diversity. *Proc Natl Acad Sci U S A* **114**, E8865-E8874, doi:10.1073/pnas.1618916114 (2017).
32 Im, S. J. *et al.* Defining CD8+ T cells that provide the proliferative burst after PD-1 therapy. *Nature* **537**, 417-421, doi:10.1038/nature19330 (2016).
33 Cornberg, M. *et al.* Clonal exhaustion as a mechanism to protect against severe immunopathology and death from an overwhelming CD8 T cell response. *Front Immunol* **4**, 475, doi:10.3389/fimmu.2013.00475 (2013).
34 Frebel, H. *et al.* Programmed death 1 protects from fatal circulatory failure during systemic virus infection of mice. *J Exp Med* **209**, 2485-2499, doi:10.1084/jem.20121015 (2012).

Materials and methods:

Mice: P14 TCRαβ transgenic mice were kindly provided by A. Oxenius (Zurich, Switzerland)[1] and Vβ5 TCRβ-only transgenic mice[2] by P. Fink (Seattle, USA). Nr4a1-EGFP reporter mice were purchased from Jaxson Laboratories[3]. C57BL6/N_Tox$^{tm1a(KOMP)Wtsi}$ founder mice were obtained from the KOMP[4] repository and crossed with a FLP deleter strain to eliminate the LacZ reporter construct and to convert them into Tox$^{tm1c(KOMP)Wtsi}$ mice. The progeny were crossed with Mx-Cre or CD4-Cre, Rosa26-stop-EYFP (Jackson laboratories), and P14 transgenic mice and afterwards intercrossed to generate Tox$^{tm1c(KOMP)Wtsi}$_x_Mx-Cre_x_Rosa26-stop-EYFP_x_P14 or Tox$^{tm1c(KOMP)Wtsi}$_x_CD4-Cre_x_Rosa26-stop-EYFP_x_P14 quadruple transgenic mice. In addition, Tox$^{tm1c(KOMP)Wtsi}$_x_ gzmBCreER^{T2} were generated. Mx-Cre_x_Rosa26-stop-EYFP_x_ P14, CD4-Cre_x_Rosa26-stop-EYFP_x_ P14, or gzmBCreER^{T2} mice were used as genetically matched controls.

Mice were bred and maintained in SPF facilities and infected in modified-SPF animal facilities initially at the University of Lausanne in Switzerland and later at the Technical University of Munich in Germany. Experiments were performed in at least six-week-old mice in compliance with the Institutional and governmental regulations in Switzerland and Germany and were approved by the responsible veterinarian authorities of the Swiss Canton Vaud and the "Regierung von Oberbayern" in Germany.

Purification of mouse T-cells, adoptive cell transfers: Tox$^{tm1c(KOMP)Wtsi}$_x_Mx-Cre_x_Rosa26-stop-EYFP_x_P14 quadruple transgenic donor mice and Mx-Cre_x_Rosa26-stop-EYFP_x_ P14 control donor mice were treated with 200µg of PolyIC (Sigma, Germany) 2-7 days before cell

harvest to induce Cre mediated excision of the 5th exon of Tox and to turn on the YFP reporter. Single cell splenocyte suspensions were obtained from these and all other T-cell donor mice by mashing total spleens through a 100 µm nylon cell strainer (BD Falcon) and red blood cells were lysed with a hypotonic ACK buffer. CD8$^+$ T-cells were isolated using the mouse CD8$^+$ T-cell enrichment kit (Miltenyi Biotech, Bergisch-Gladbach, Germany) **and sorted for YFP positive T cells**. 2-5x10^3 CD45.1$^+$ congenic naïve wt or ToxΔ^{Ex5} P14αβ transgenic T-cells were transferred into naïve CD45.2$^+$ hosts. Given the mixed C57BL6/N and C57BL6/J background of the donor mice, we obtained C57BL6/N and C57BL6/J from Charles River (France) and used the F1 offspring as hosts for adoptive T-cell transfers. T-cell response kinetics and some phenotyping experiments were performed upon co-transferring congenic wt and ToxΔ^{Ex5} P14αβ transgenic T-cells into C57BL/6NxJF1 or Vβ5 hosts and ratios of ToxΔ^{Ex5} over wt P14 T-cells were determined within the same host mouse. P14αβ T-cells were re-isolated from infected mice through magnetic cell separation, using anti-CD45.1 biotinylated antibody and anti-biotin microbeads (Miltenyl Biotech, Bergisch-Gladbach, Germany).

Infections: Frozen LCMV stocks were diluted in PBS and 2x10^5 PFU LCMV Armstrong were injected intraperitoneally. Chronic LCMV clone-13 was injected intravenously. The C6 strain of LCMV clone-13, which expresses a low affinity altered peptide ligand for P14 T-cells, was described previously[5] and 5x10^6 PFU were injected per mouse. The previously descried mixed-mutant infections[5] were performed by co-injecting a mixture of a gp33 deficient LCMV clone-13 mutant (A3 strain, encoding an H-2Db binding deficient gp33 altered peptide ligand[6]) along with wild-type LCMV clone-13. In initial experimental series performed at the University of Lausanne in Switzerland, we used a total dose of LCMV clone-13 of 2x10^6 PFU per mouse. For the mixed infection we used 1.33x10^6 PFU gp-33 deficient (A3 APL) LCMV clone-13 and

$0.66x10^6$ PFU wt LCMV clone-13. After the relocation of the laboratory to the Technical University of Munich, Germany, which involved the usage of a different animal facility, we had to slightly increase the total dose to $5x10^6$ PFU and we used $4,5x10^6$ PFU gp-33 deficient LCMV clone-13 and $0.5x10^6$ PFU wt LCMV clone-13 for the mixed infection. To determine virus load, blood samples or splenocyte suspensions were shock frozen to release the virus. Diluted samples were used to infect Vero cells and virus titers were determined using the LCMV focus forming assay[7].

Tamoxifen treatment and Tox gene deletion assessment: Mice were treated with 2mg of Tamoxifen (Sigma Aldrich) dissolved in corn oil (Sigma Aldrich) from day 20 to 25 post LCMV clone-13 infection. To assess the effective deletion of TOX, tetramer-positive cells from infected mice were sorted and DNA isolated with QIAamp DNA Micro Kit (Qiagen). The extracted DNA was amplified with TCATGAAGCCCAAACAGGACAGTGC and GTAGGGAAGGGACAAGGATAACAAC primers and the KAPA Mouse Genotyping Kit (Kapa Biosystems) to have a genomic Wt band at 1673 bp and in exon 5-deleted cells a band at 814 bp. Note that the fragment length includes introns.

Surface and intracellular antibody staining and flow cytometry cell sorting of mouse cells: Surface staining was performed for 30 min at 4°C in RPMI-1640 media (Sigma Aldrich) supplemented with 2% FCS (Sigma Aldrich) and 0.01% azide (Sigma Aldrich) (FACS buffer) using the following antibodies: anti-CD8a (53-6.7), CD45.1 (A20), CD45.2 (104), PD-1 (RMP1-30), Klrg1 (2F1), CD127 (eBioSB/199), CD62L (MEL-14), TOX (TXRX10), Tbet (4B10), Eomes (Dan11mag); Tim3 (RMT3-23), TCRβ (H57-597), CD5 (53-7.3), CD69 (H1.2F3) from Biolegend, APC conjugated-gp33 tetramer (TCMetrix). For detection of EdU, the Click-iT® EdU Alexa

Fluor® 647 Flow Cytometry Assay Kit (Thermo Fisher) was used. Cells were washed twice and fixed in PBS supplemented with 1% formaldehyde, 2% glucose and 0.03% azide for 20 min. Then the cells were washed again and resuspended in FACS buffer. For intracellular cytokine staining, splenocytes were re-stimulated in vitro with gp33-41 (gp33) peptide (5mM) for 5h in the presence of Brefeldin A (7 µg/ml) for the last 4.5 h, fixed and permeabilized, using the Cytofix/Cytoperm Kit (BD) and stained with mAbs for IFNγ (XMG1.2), TNF (MP6-XT22). Intracellular transcription factor staining was performed with the Foxp3 / Transcription Factor Staining kit (eBioscience) and stained with anti-TCF-1 (S33966, BD Pharmingen), TOX (TXRX10, eBioscience), Eomes (Dan11mag), and T-bet (eBio4B10, both from eBioscience). For flow cytometry sorting, living cells were stained in 2% FCS RPMI media and sorted on a FACSAriaFusion instrument (BD). Flow cytometry measurements of cells were performed on an LSR-Fortessa flow cytometer (BD). All data were analyzed using FlowJo (TreeStar).

Retroviral transduction of CD8 T-cells: Retroviral supernatant was produced from Phoenix E cells transfected with FuGENE® 6 (Promega) with retroviral expression plasmids (pMSCV) containing either an IRES-GFP or gene of interest-IRES-GFP expression cassette. TOX sequence was custom synthesized by GenScript in codon optimized form and cloned into the pMSCV vector. Nr4a1 was amplified from activated CD8 T-cells cDNA template with primers FW: ACTGCTCGAGGTGGGAGCCGGCTGGAGATG and REV: ACTGGAATTCGGGCAGGGGTCA GAAAGACAATGTG. The vector pMIG-IRF4 was obtained from Addgene (plasmid # 58987)[8]. For retroviral transduction, naive $CD8^+$ T-cells were isolated from spleens of P14αβ TCR transgenic mice and activated in vitro with Mouse *T-Activator CD3/CD28 Dynabeads* (Gibco by Thermo Fisher Scientific, Carlsbad,USA) in the presence of recombinant human IL-2 (30 U/ml, Chiron) for 24 hours before spin transduction with viral supernatants in the presence of

0.8 mg/ml polybrene. After 24 hours, $5x10^4$ P14 transduced with empty or TOX vector were transferred into recipient Vb5 mice, which were infected with the mix LCMV clone-13 infection ($4.5x10^6$ PFU gp-33 deficient clone-13 plus $0.5x10^6$ PFU wt LCMV clone-13). $CD8^+$ T-cells transduced with empty, Tox, Nr4a1 and IRF-4 vector were kept in culture for several days with RPMI media supplemented with 10 % FCS and 50 U/ml of recombinant human IL-2 (Chiron).

Cryosections and staining of spleens: Spleens from chronically infected mice (8 or 14 days p.i.) were harvested and fixed in paraformaldehyde (4 %) for 4 h. After transfer into 30 % sucrose solution and equilibration overnight, the organs were embedded in OCT-tissue Tek and frozen immediately over liquid nitrogen. The organs were then stored at -80 °C. Sections with 5 µm of thickness were cut using the microtome cryostat (Microm HM 505 E Cryostat, GMI) at a temperature between -20 and -25°C. The sections were air-dried and fixed in -20 °C cold acetone for 5 min. For the staining, the sections were dehydrated with PBS for 5 min at room temperature, blocked and incubated with CD3 (17A2), CD45.R/B220 (RA3-6B2) and CD45.1 (A20) from Biolegend for 4 h in the dark at 4 °C. The slides were mounted with Prolong Gold mounting buffer (Fisher Scientific) and cover slipped. Images were acquired with Leica DMi8 fluorescent microscope (Leica Microsystems) that is configurated to work as a fully automated slide scanner. The whole spleen or a representative part was scanned in high resolution using the LAS X Navigator (Leica Microsystems). Afterwards, the images of different channels were merged and the images exported for analysis. Processing and first steps of analysis of the images was performed using ImageJ. Subsequently, an R-script was used to vectorize the sections. Based on density threshold of the CD3 and B220 fluoresces signal, the

compartments of the spleen (red-pulp versus B- and T-Cell zone of the white-pulp) was assessed. The relative distribution of P14 T-cells in these compartments was then determined.

Organs histological evaluation: On day 12 after 5* 10^6 PFU LCMV clone-13 infection, lungs and livers from mice that receive 10^4 wt or ToxΔ^{Ex5} P14 T-cells were collected, fixed in 10% neutral buffered formaldehyde, and paraffin embedded. Tissue sections (5 µm) were stained with H&E and analyzed microscopically. Scoring of lung pathology by a pathologist blinded to the experimental design was graded based on a previously described scale [9,10] as follows: 1) mild interstitial mononuclear infiltrates, disorganized BALT, and perivascular edema; 2) moderate interstitial mononuclear infiltrates, small amount of organized BALT, and pulmonary edema; 3) moderate interstitial mononuclear infiltrates, pulmonary edema, enhanced organized BALT, mild bronchiolization, and mild consolidation; 4) severe interstitial mononuclear infiltrates, greatly enhanced pulmonary edema, enhanced organized BALT, moderate bronchiolization, moderate consolidation, and moderate necrotizing bronchiolitis; 5) severe interstitial mononuclear infiltrates, greatly enhanced pulmonary edema, enhanced organized BALT, severe bronchiolization, severe consolidation, severe necrotizing bronchiolitis, and vasculitis involving more than half of the lung. The histology photographs showing representative high power views of a small portion of one lobe of the lung demonstrate examples of the types of pathology observed in different treatment groups. Liver histology was evaluated by an experienced pathologist blinded to the experimental design with respect to the parameters of the Ishak score and the alterations described by Cornberg et al. (periportal and sinusoidal infiltration and hepatocellular necrosis) as well as the distribution and pattern of infiltrating T-cells[11]. For the determination of necrosis foci in the liver, the slides were digitalized with a scanning system (Leica AT2, Wetzlar, Germany) and

number of foci of necrosis were count on a whole section of one liver lobe and normalized to number of necrosis per cm^2.

Human HCV-specific $CD8^+$ T-cells: HLA-A*02-positive (HLA-A*02^+) subjects with chronic HCV infections; spontaneously cleared HCV infections; HCV infections cleared through Harvoni [Gilead Sciences], Sovaldi [Gilead Sciences]/Daklinza [BMS], or Viekirax/Exviera [AbbVie] treatment; and healthy control donors (attending the University Hospital of Freiburg were included in the study). In detail: 5 patients, all not in the acute phase and unknown time post infection were used as healthy control; 5 patients, of which 3 had HCV infection more than 5 years ago and 2 presumably more than 2 years ago, were chosen as spontaneously cleared donors; 6 patients, all 24 weeks after the end of therapy (36 weeks after therapy initiation); of which 5 have been chronically HCV-infected for more than 20 years and one is not precisely known but presumably at least for 10 years, were taken as cleared donors; 6 patients, of which 4 cleared the infection most probably more than 20 years ago and 2 unknown time but presumably at least since 10 years, were taken as spontaneously cleared donors.

Written informed consent was obtained in all cases, and the study was conducted in accordance with federal guidelines, local ethics committee regulations, and the Declaration of Helsinki (1975). Approval was obtained from the ethics committee of the Albert-Ludwigs-Universität, Freiburg, Germany (HBUF; 474/14). Peripheral blood mononuclear cells (PBMCs) were isolated from EDTA-anticoagulated blood by density gradient centrifugation. Peptide-MHC class I tetramer-based enrichment procedures were performed as described previously [12]. $CD8^+$ T-cell subset in healthy donors were defined based on CD45RA and CCR7 surface (mAb clones: HI100 and G043H7, respectively). Peptides of HLA-A*02-restricted HCV-derived epitopes, influenza virus (FLU)-derived epitope were obtained from Genaxxon. Peptides were

dissolved in dimethyl sulfoxide (Sigma, Germany) at 20 mg/ml and diluted in complete medium to 1mg/ml before usage. Major histocompatibility complex (MHC) class I epitope-specific tetramers were generated by conjugation of biotinylated peptide-MHC class I monomers with PE- or APC conjugated streptavidin at a MHCI:Strepatividin molar ratio of 5:1. The following reagents were used for multi-parametric flow cytometry: anti-HLA-A*02 (BB7.2, BD), anti-CD45RA (HI100, BD), anti-Tox (TXRX10, eBioscience), anti-CCR7 (G043H7, BioLegend), anti-PD1 (EH12.2H7, BioLegend), anti-TCF1 (C63D9, Cell Signalling), anti-CD8 (RPA-T8, BD). 7-AAD (BD Biosciences) was used for live/dead discrimination. FoxP3/Transcription Factor Staining Buffer Set (eBioscience) was applied according to the manufacturer's instructions to stain for nuclear molecules. Cells were fixed with paraformaldehyde (2% PFA) before sample acquisition on LSRFortessa (BD Biosciences).

Overexpression of Tox in human T-cells: Human PBLs used in this study were from healthy donors from the Israeli Blood Bank (Tel-Hashomer, Israel) after obtaining an informed consent. For virus production, transfection of 2×10^6 293GP cells with 9µg DNA of retroviral constructs encoding TOX-IRES-GFP genes and 4.5µg envelop plasmid (VSV-G) was performed using JetPrime transfection reagent (Polyplus, France)[13]. Retroviral supernatant was collected 36 h after the DNA transfection. Freshly isolated human PBLs from healthy donor were stimulated for 48 h in the presence of 50ng/ml OKT3 (eBioscience, San Diego, CA) before transduction. Following stimulation, lymphocytes were transduced with retroviral vectors by transfer to non-treated tissue culture dishes (Nunc, Rochester NY) that had been pre-coated with RetroNectin (Takara, Japan) and retroviral vectors as previously described[14]. Lymphocytes were cultured in BioTarget medium (Biological Industries, Beth Haemek, Israel), 10% FBS and 300 IU/ml IL-2. $CD8^+$ T-cells were stained with anti-PD-1 antibody (EH12.2H7,

Biolegend) and analyzed by flow cytometry. For IFNγ and TNF measurements, $CD8^+$ T-cells were transduced with the MART1 specific TCR F4-TCR and/or TOX gene and re-stimulated for 16 hours in presence of SK-MEL-23 and 888-A2 cells and analyzed with DuoSet® ELISA Development Systems (R&D). Backgroud TNF and IFNγ production was determined by co-culturing control and TOX transduced cells, which do not contain the F4 TCR, with SK-Mel-23. Background values were subtracted from the aforementioned measurement.

Microarrays: Sorted and frozen P14 T-cells were sent to IMGM Laboratories to generate Microarray gene expression profiles. Agilent mouse GE v2 Microarrays (4x44K) (for Array 1) and Agilent SurePrint G3 Mouse Gene expression 8x60KK Microarrays (for Array 2) were used in combination with a one-color based hybridization protocol and was performed as described in the manufacturer's instructions. Signals on the microarrays were detected using the Agilent DNA Microarray Scanner (Scan Control A.8.4.1 Software, Agilent Technologies) and analyzed with Feature Extraction Software 10.7.3.1 (Agilent Technologies) using default parameters (protocol GE1-107_Sep09 and Grid: 028005_D_F_20130207. GeneSpring GX12 (for Supp. Fig 1A) and GeneSpring GX13.0 (for Supp. Fig 1B) (Agilent Technologies) was used to normalize and analyze the raw data as well for quality control.

Microarray analysis: Statistical analysis for microarray data was performed using limma (version 3.34.9)[15]. Values were corrected by 'saddle normexp'[16], normalized by 'Quantile' method[17] and log2-transformed for the downstream analysis.

Next generation sequencing (NGS): At day 8 or 20 post infection, splenocytes were enriched for $CD45.1^+$ P14 T-cells using biotin labelled ant-CD45.1 antibodies and anti-biotin conjugated

microbeads in combination with magnetic MACS cell separation (Miltenyi Biotech, Bergisch-Gladbach, Germany). High purity (>95%) untouched samples were then obtained by flow cytometry based sorting for GFP^+ $CD45.1^+$ P14 cells. The cells were lysed and RNA was extracted using the Agencourt RNAdvance Cell v2 kit (A47942, Beckman Coulter). RNA integrity number (RIN) and yield were assessed using RNA 6000 Pico Kit (5067-1513, Agilent). Only samples with RIN>8 were used for downstream cDNA synthesis and library preparation. cDNA synthesis and PCR amplification using 1 ng of total RNA from each sample was performed using SMART-Seq v4 Ultra Low Input RNA Kit for Sequencing (634891, Takara/Clontech). After cDNA synthesis, each sample was subjected to 12 cycles of PCR amplification. The generated amplicons were assessed and their concentration was determined with the use of Agilent High Sensitivity DNA Kit (5067-4626, Agilent). 150 pg of the resulting amplified cDNA were used for library preparation with the Illumina Nextera XT DNA Library reagents (FC-131-1024, Illumina). After PCR amplification of the fragmented libraries, the samples were purified with (0.6x) Agencourt AMPure XP beads and eluted in 10 µl of molecular grade water. The quality of the resulting library was assessed with the use of Agilent High Sensitivity DNA Kit (5067-4626, Agilent). The library quantification was performed based on the Illumina recommendations (SY-930-1010, Illumina) with the use of KAPA SYBR FAST qPCR Master Mix (KK4600, Kapa Biosystems). The samples were sequenced on Illumina HiSeq 2500 system at the following conditions - rapid run, 100 base pairs single-end read, dual-indexed sequencing resulting in 20 million reads per sample.

NGS data processing: Reads were processed using snakemake pipelines[19] as indicated under (https://gitlab.lrz.de/ImmunoPhysio/bulkSeqPipe). Sequencing quality was assessed with fastqc[20], filtering was performed by trimmomatic v0.36[21] using, mapping by STAR v2.5.3a[22]

with genome Mus_musculus.GRCm38, counting by htseq v0.9.1[23] with annotation Mus_musculus.GRCm38.91. To supervise STAR and fastqc results we used multiqc v1.2[24]. All used parameters and adapters can be found at (https://gitlab.lrz.de/ ImmunoPhysio/alfei_tox.

NGS data analysis: Genes with total reads lower than 10 across all the samples were removed before comparisons. Differential expression analysis was performed with methods based on the negative binomial distribution in DESeq2 (version 1.18.1)[25], using default parameters. Read counts were modelled as a negative binomial distribution with estimated mean values and gene-specific dispersion parameters; each gene was fitted as a generalized linear model (GLM); Wald statistics and Benjamini & Hochberg (BH)[18] were used for significance test and multiple comparisons.

Heatmap visualization: For heatmaps, genes were selected from differentially expressed gene lists of ToxΔ^{Ex5} Vs Tox wt at different time points. Genes highlighted by an asterix were selected for illustrative purposes even though their adjusted p-value was above 0.05. Pheatmap (version 1.0.10)[26] was used for the heatmap visualization, colors represent the Z-score derived from the normalized, log2 transformed expression values obtained from DESeq2 (version 1.18.1)[25].

ATAC sequencing: $2*10^3$ wt or ToxΔ^{Ex5} P14 T-cells were transferred into C57BL6 host, infected with $2x10^5$ PFU LCMV Armstrong or $5x10^6$ PFU LCMV-c13 or $5x10^6$ PFU LCMV mixed c13 infection and collected on day 8 (for LCMV-c13 infection) or day 13 (LCMV Armstrong, LCMV-c13 and LCMV mixed c13 infection). P14 T-cells were isolated and FACS-sorted, before being

frozen in freezing media (RPMI with 10% FCS and 10 % DMSO). The samples were shipped to Quick Biology Inc. Pasadena, California, US for the sample extraction, ATAC-seq Library preparation and sequencing. The sequencing has been done with HiSeq 4000, with ~60M total reads/sample, 30M pairs. Pair-end reads quality were accessed with TrimGalore, low quality bases and adaptors were trimmed by TrimGalore. The reads were then mapped to GRCm38 by BWA-0.5.9. Reads mapped to mitochondrial genome or reads from PCR duplicates were removed. 5' of reads aligned to the positive and negative strands are offset by +4 bp and -5 bp, respectively. Only reads in nucleosome-free bin (fragment length between 38 and 100 bp) are used for downstream analysis. ATAC-seq peaks were called with MACS2[27].

Gene Transcription Regulation Database (GTRD): The following slightly edited information was obtained from the providers webpage. 'A collection of uniformly processed ChIP-sequencing data based on the BioUML platform, was used to identify transcription factors that bind to Tox gene. ChIP-seq experiment information were collected in semi-automated way from literature, GEO and ENCODE. Raw ChIP-seq data in the form of fastq and SRA files were fetched from ENCODE and SRA databases. Sequenced reads were aligned using Bowtie2 [28]aligner. ChIP-seq peaks were called using 4 different methods: MACS[27], SISSRS[29], GEM[30], and PICS[31] . Clusters for the same TF revealed by different peak calling methods were joined into metaclusters. Metaclusters represent non-redundant set of transcription factor binding sites. The clustering algorithm used in GTRD is described in the main GTRD paper [32,33].' Thank to this database, we were able to identify all the known transcription factors that bind to the Tox gene. Moreover, we run the exported fine on the Integrative Genomic Viewer (IGV, Broad Institute and the Regents of the University of California) to create a snapshot of the binding site of selected transcription factors illustrated in Supplementary Figure 8.

Genome-Wide and Loci-Specific Methylation Analysis: Naïve and P14 CD8 T-cells were sorted from the splenocytes of acutely or chronically infected mice. DNA was isolated by using the QIAGEN DNeasy kit. Genomic DNA was bisulfite treated using the EZ DNA methylation kit (Zymo Research). Bisulfite-induced deamination of cytosine allows for sequencing-based discrimination of methylated versus non-methylated cytosine[34]. Whole-genome bisulfite DNA methylation sequencing was performed as previously described (you may cite one of Youngblood's recent papers-e.g., Nature, Cell, JEM, 2017). Briefly, bisulfite-modified DNA-sequencing libraries were generated using the EpiGnome kit (Epicentre) per the manufacturer's instructions and were sequenced using an Illumina HiSeq system. Sequencing data were aligned to the mm10 genome by using BSMAP[35]. Differentially methylation analysis of CpG methylation among the datasets was determined with a Bayesian hierarchical model to detect regional methylation differences with at least three CpG sites[36]. For locus-specific methylation analysis, the bisulfite-modified DNA was PCR amplified using *Tox* locus-specific primers (forward primer :5'-GTGTAAGTTATTGTGATTCTGATTGTG-3', reverse primer 5'-CTTTAACTACCCTCTCTAAATTAA AAAACC-3'). The PCR amplicon was cloned into the pGEM-T TA cloning vector (Promega) and then transformed into XL10-Gold ultracompetent E. coli bacteria (Stratagene). Individual bacterial colonies were grown overnight over Luria-Bertani (LB) agar containing ampicillin (100 mg/L), X-gal (80 mg/L), and IPTG (20 mM). White colonies were selected and subcultured into LB broth with ampicillin (100 mg/L) overnight; the cloning vector was purified; and the genomic insert was sequenced.

General data Analyses: Bar graphs depict the mean ± SEM or ± SD as indicated. Statistical analyses were performed with Prism 7.0 (Graphpad Software). Non-paired t tests (two-tailed)

were used according to the type of experiments. p values < 0.05 were considered significant (*p < 0.05; **p < 0.01; ***p <0.001); p values > 0.05 were non-significant (ns).

Ingenuity Pathway Analysis (IPA, Qiagen): Version 46901286 (between 02-03/2019) was used to further analyze the high content gene array or next generation sequencing data. Differential gene expression data for the pure versus mixed mutant LMCV infection (Supp. Fig. 1A), the day8 Wt versus ToxΔ^{Ex5} (Fig. 2E), day 8 Wt versus ToxΔ^{Ex5} for Tim3^{+} and Tim3^{-} populations were obtained though the above described pipeline were loaded into IPA. NGS datasets were filtered for p-values ≤0.05 and MeanExpression ≥50 and for microarray data for p-values ≤0.05 and AveExpression ≥6 . Log2-FC cutoffs were adjusted to obtain between 1000-1500 DEG and values of >|0.5| for NGS and >|0.3| for microarray data were used. "Core-analysis" were performed for all datasets. Out of these, pathway activity analysis and upstream regulators were extracted. Specific data comparisons and visualizations were performed as indicated in the supplementary figure legends and by using data linking options provided by the software.

References:

1 Pircher, H., Burki, K., Lang, R., Hengartner, H. & Zinkernagel, R. M. Tolerance induction in double specific T-cell receptor transgenic mice varies with antigen. *Nature* **342**, 559-561, doi:10.1038/342559a0 (1989).

2 Dillon, S. R., Jameson, S. C. & Fink, P. J. V beta 5+ T cell receptors skew toward OVA+H-2Kb recognition. *J Immunol* **152**, 1790-1801 (1994).

3 Moran, A. E. *et al.* T cell receptor signal strength in Treg and iNKT cell development demonstrated by a novel fluorescent reporter mouse. *J Exp Med* **208**, 1279-1289, doi:10.1084/jem.20110308 (2011).

4 Koscielny, G. *et al.* The International Mouse Phenotyping Consortium Web Portal, a unified point of access for knockout mice and related phenotyping data. *Nucleic Acids Res* **42**, D802-809, doi:10.1093/nar/gkt977 (2014).

5 Utzschneider, D. T. *et al.* High antigen levels induce an exhausted phenotype in a chronic infection without impairing T cell expansion and survival. *J Exp Med* **213**, 1819-1834, doi:10.1084/jem.20150598 (2016).

6 Puglielli, M. T. *et al.* In vivo selection of a lymphocytic choriomeningitis virus variant that affects recognition of the GP33-43 epitope by H-2Db but not H-2Kb. *J Virol* **75**, 5099-5107, doi:10.1128/JVI.75.11.5099-5107.2001 (2001).

7 Utzschneider, D. T. *et al.* T cells maintain an exhausted phenotype after antigen withdrawal and population reexpansion. *Nat Immunol* **14**, 603-610, doi:10.1038/ni.2606 (2013).

8 So, A. Y. *et al.* Dual mechanisms by which miR-125b represses IRF4 to induce myeloid and B-cell leukemias. *Blood* **124**, 1502-1512, doi:10.1182/blood-2014-02-553842 (2014).

9 Wlodarczyk, M. F., Kraft, A. R., Chen, H. D., Kenney, L. L. & Selin, L. K. Anti-IFN-gamma and peptide-tolerization therapies inhibit acute lung injury induced by cross-reactive influenza A-specific memory T cells. *J Immunol* **190**, 2736-2746, doi:10.4049/jimmunol.1201936 (2013).

10 Chen, H. D., Fraire, A. E., Joris, I., Welsh, R. M. & Selin, L. K. Specific history of heterologous virus infections determines anti-viral immunity and immunopathology in the lung. *Am J Pathol* **163**, 1341-1355, doi:10.1016/S0002-9440(10)63493-1 (2003).

11 Cornberg, M. *et al.* Clonal exhaustion as a mechanism to protect against severe immunopathology and death from an overwhelming CD8 T cell response. *Front Immunol* **4**, 475, doi:10.3389/fimmu.2013.00475 (2013).

12 Nitschke, K. *et al.* Tetramer enrichment reveals the presence of phenotypically diverse hepatitis C virus-specific CD8+ T cells in chronic infection. *J Virol* **89**, 25-34, doi:10.1128/JVI.02242-14 (2015).

13 Eisenberg, V. *et al.* Targeting Multiple Tumors Using T-Cells Engineered to Express a Natural Cytotoxicity Receptor 2-Based Chimeric Receptor. *Front Immunol* **8**, 1212, doi:10.3389/fimmu.2017.01212 (2017).

14 Tal, Y. *et al.* An NCR1-based chimeric receptor endows T-cells with multiple anti-tumor specificities. *Oncotarget* **5**, 10949-10958, doi:10.18632/oncotarget.1919 (2014).

15 Ritchie, M. E. *et al.* limma powers differential expression analyses for RNA-sequencing and microarray studies. *Nucleic Acids Res* **43**, e47, doi:10.1093/nar/gkv007 (2015).

16 Silver, J. D., Ritchie, M. E. & Smyth, G. K. Microarray background correction: maximum likelihood estimation for the normal-exponential convolution. *Biostatistics* **10**, 352-363, doi:10.1093/biostatistics/kxn042 (2009).

17 Bolstad, B. M., Irizarry, R. A., Astrand, M. & Speed, T. P. A comparison of normalization methods for high density oligonucleotide array data based on variance and bias. *Bioinformatics* **19**, 185-193 (2003).

18 Benjamini, Y. & Hochberg, Y. Controlling the false discovery rate: a practical and powerful approach to multiple testing. *Journal of the royal statistical society. Series B* 289-300 (1995).

19 Koster, J. & Rahmann, S. Snakemake--a scalable bioinformatics workflow engine. *Bioinformatics* **28**, 2520-2522, doi:10.1093/bioinformatics/bts480 (2012).

20 S, A. FastQC: a quality control tool for high throughput sequence data. . *http://www.bioinformatics.babraham.ac.uk/projects/fastqc* (Version: 0.11.6).

21 Bolger, A. M., Lohse, M. & Usadel, B. Trimmomatic: a flexible trimmer for Illumina sequence data. *Bioinformatics* **30**, 2114-2120, doi:10.1093/bioinformatics/btu170 (2014).
22 Dobin, A. *et al.* STAR: ultrafast universal RNA-seq aligner. *Bioinformatics* **29**, 15-21, doi:10.1093/bioinformatics/bts635 (2013).
23 Anders, S., Pyl, P. T. & Huber, W. HTSeq--a Python framework to work with high-throughput sequencing data. *Bioinformatics* **31**, 166-169, doi:10.1093/bioinformatics/btu638 (2015).
24 Ewels, P., Magnusson, M., Lundin, S. & Kaller, M. MultiQC: summarize analysis results for multiple tools and samples in a single report. *Bioinformatics* **32**, 3047-3048, doi:10.1093/bioinformatics/btw354 (2016).
25 Love, M. I., Huber, W. & Anders, S. Moderated estimation of fold change and dispersion for RNA-seq data with DESeq2. *Genome Biol* **15**, 550, doi:10.1186/s13059-014-0550-8 (2014).
26 Kolde, R. https://cran.r-project.org/web/packages/pheatmap/index.html.
27 Zhang, Y. *et al.* Model-based analysis of ChIP-Seq (MACS). *Genome Biol* **9**, R137, doi:10.1186/gb-2008-9-9-r137 (2008).
28 Langmead, B. & Salzberg, S. L. Fast gapped-read alignment with Bowtie 2. *Nat Methods* **9**, 357-359, doi:10.1038/nmeth.1923 (2012).
29 Narlikar, L. & Jothi, R. ChIP-Seq data analysis: identification of protein-DNA binding sites with SISSRs peak-finder. *Methods Mol Biol* **802**, 305-322, doi:10.1007/978-1-61779-400-1_20 (2012).
30 Guo, Y., Mahony, S. & Gifford, D. K. High resolution genome wide binding event finding and motif discovery reveals transcription factor spatial binding constraints. *PLoS Comput Biol* **8**, e1002638, doi:10.1371/journal.pcbi.1002638 (2012).
31 Zhang, X. *et al.* PICS: probabilistic inference for ChIP-seq. *Biometrics* **67**, 151-163, doi:10.1111/j.1541-0420.2010.01441.x (2011).
32 Yevshin, I., Sharipov, R., Valeev, T., Kel, A. & Kolpakov, F. GTRD: a database of transcription factor binding sites identified by ChIP-seq experiments. *Nucleic Acids Res* **45**, D61-D67, doi:10.1093/nar/gkw951 (2017).
33 Yevshin, I., Sharipov, R., Kolmykov, S., Kondrakhin, Y. & Kolpakov, F. GTRD: a database on gene transcription regulation-2019 update. *Nucleic Acids Res* **47**, D100-D105, doi:10.1093/nar/gky1128 (2019).
34 Trinh, B. N., Long, T. I. & Laird, P. W. DNA methylation analysis by MethyLight technology. *Methods* **25**, 456-462, doi:10.1006/meth.2001.1268 (2001).
35 Xi, Y. & Li, W. BSMAP: whole genome bisulfite sequence MAPping program. *BMC Bioinformatics* **10**, 232, doi:10.1186/1471-2105-10-232 (2009).
36 Feng, H., Conneely, K. N. & Wu, H. A Bayesian hierarchical model to detect differentially methylated loci from single nucleotide resolution sequencing data. *Nucleic Acids Res* **42**, e69, doi:10.1093/nar/gku154 (2014).

Supplementary Figure legends

Supplementary Figure 1 – **Gene expression signatures of dysfunctional T-cells. A,** C57BL/6 mice engrafted with $2x10^3$ P14 T-cells were infected with $2x10^6$ PFU wt clone-13 or $0.4x10^6$ PFU wt clone-13 mixed with $1.6x10^6$ PFU gp33-deficient LCMV clone-13 mutant strain. P14 were re-isolated on day 28, purified using flow cytometry-based sorting, and the transcriptional profile was analyzed using RNA microarrays. The volcano plot graphs Log_2 FC against the p-values. Dashed vertical and horizontal lines reflect the filtering criteria (Log_2 FC ≥ |0.5| and p-value ≤ 0.05). The number of genes that match the filter criteria are highlighted in yellow or green. The list on the right shows top differentially expressed genes with Log_2 FC ≥ |2| p-value ≤ 0.05. **B,** C57BL/6 mice were engrafted with $2x10^3$ P14 T-cells and subjected to a primary LCMV Armstrong or clone-13 infection. 4 weeks later the P14 T-cells were re-isolated and transferred into naïve host mice which were infected by LCMV Armstrong. 8 days later, cells were harvested and analyzed, and graphically illustrated as explained in A. **C**, datasets from A and B were filtered for AverageExpression >6, Log_2 FC ≥ |0.5| and p-value ≤ 0.05. Top, the venn diagram shows the overlap beween both datasets. The graph at the bottom plots foldchange values from dataset B (x-axis) versus dataset A (y-axis), colored dots indicate genes with Log_2 FC ≥ |2|.

Supplementary Figure 2 – TOX expression increases with positive selection in the thymus. A, Gating strategy, thymocytes were collected from 5 weeks old C57BL/6 mice and stained for CD4, CD8, CD5, CD69, and Tox expression. Gates were applied to stratify the $CD8^{bright}$ $CD4^{bright}$ population (upper gate), which preferentially contains pre-selection thymocytes, from the

$CD8^{dull}$ $CD4^{dull}$ population (lower gate), which contains cells that underwent positive selection. Additional gating was applied to improve the separation of preselection $CD5^{low}$ $CD69^{low}$ cells from positively selected cells with upregulated CD69 and CD5 expression. High levels of Tox expression were found among positively selected $CD5^{high}$ $CD69^{high}$ cells while $CD5^{low}$ $CD69^{low}$ cells showed no or minimum levels of Tox.

B, Tox MFI data for 4 mice. Horizontal bars represent the mean; unpaired t tests were performed with *<0.05; **p < 0.01; ns = not significant (p > 0.05).

Supplementary Figure 3 – Wt and Tox deficient T-cells become similarly activated but show distinct phenotypes even in mice with high LCMV virus titers. A, $Tox^{tm1c(KOMP)Wtsi}$_x_CD4-Cre_x_Rosa26-stop-EYFP_x_P14 and CD4-Cre_x_Rosa26-stop-EYFP_x_P14 mice were directly infected with $5x10^6$ PFU clone-13. Spleens were collected 2.5 days post infection. Shown are representative plots of CD69 expression by P14 T-cells and corresponding frequency data for all mice. **B**, PD-1 expression measured and illustrated as described in A. **C-E**, $1x10^4$ wt and $Tox\Delta^{Ex5}$ P14 T-cells from polyIC treated donors (as described in figure 2) were transferred into Vβ5 or C57BL/6 host mice which were infected with $5x10^6$ PFU LCMV clone-13 and analyzed on day 8 or day 20 post infection. Representative histograms and PD-1 MFI data for $Tox\Delta^{Ex5}$ (light blue) or wt (blue) P14 T-cells, grey curve represent endogenous CD8 T-cells (**C**); representative histograms and frequency of KLRG1 expressing $Tox\Delta^{Ex5}$ and wt P14 cells (**D**); cytokine production following brief in vitro gp33 re-stimulation in the presence of Brefeldin A for $Tox\Delta^{Ex5}$ (light blue) or wt (blue) P14 T-cells (**E**). **F**, C57BL/6 mice are engrafted with $Tox\Delta^{Ex5}$ or wt P14 T-cells obtained from polyIC treated donors and hosts were infected with $5x10^6$ PFU LCMV clone-13 or $2x10^5$ PFU Armstrong. Representative flow cytometry plots and data for all

mice showing Granzyme B expression in splenic wt and ToxΔ^{Ex5} P14 T-cells on day 8 post infection. Symbols are data for individual mice; solid horizontal lines represent the mean. Unpaired t tests were performed with *<0.05; **p < 0.01; ns = not significant (p > 0.05). **G**, Virus titers in wt LCMV clone-13 infected wt and ToxΔ^{Ex5} P14 T-cell containing Vβ5 host mice at 7 days post infection in spleen, liver, and kidneys.

Supplementary Figure 4 – Late deletion of Tox fails to alter the dysfunctional T-cell phenotype. A, Tox$^{tm1c(KOMP)Wtsi}$_x_ gzmBCreER^{T2} and gzmBCreER^{T2} mice were infected with 5x10^{6} PFU clone-13 and treated with 2 mg Tamoxifen from day 20 to 25 post infection. This allows for the specific elimination of Tox in activated, granzyme B-expressing T-cells. Splenocytes were collected on day 35. **B**, Identification of gp33 tetramer-positive polyclonal T-cells. **C**, tetramer-positive cells from both types of mice were sorted, DNA extracted, and the status of Tox gene was analyzed by PCR using primers that amplify the Tox gene. The missing 5th exon covers 231 base pairs. **D** and **E**, representative histograms and MFI data for PD-1 (**D**) and KLRG-1 expression (**E**) with wt cells in light dark and ToxΔ^{Ex5} in light blue. Symbols are data for individual mice; solid horizontal lines represent the mean. Unpaired t tests were performed with *<0.05; **p < 0.01; ns = not significant (p > 0.05).

Supplementary Figure 5 – Tox impacts the expression of a large number of genes that are tightly linked to a dysfunctional phenotype. A and B, DEG lists were defined by applying AverageExpression >6, p<0.05, and Log_2 FC ≥ |0.3| as filter criteria to the datasets shown in Supp.Fig. 1A (dysfunctional versus normal T cells, red) and Supp.Fig. 1B (re-expanded dysfunctional versus re-expanded memory T cells, blue). Another DEG list was defined by

filtering the Fig. 2E dataset of day 8 Tox wt versus ToxΔ^{Ex5} T cell for MeanExpression >50, $p<0.05$, and Log_2 FC ≥ |0.3|. **A**, Venn diagram showing the overlap between the DEG. Numbers on the outside depict the DEG overlap only between two of the three data sets. **B**, The graph shows p-values by which the listed regulators are linked to the dataset in Supp.Fig. 1A (x-axis) or the dataset from Fig. 2E (y-axis). To obtain these data, the DEG list from Supp.Fig. 1A and from Fig. 2E were separately loaded into the "Ingenuity pathway analysis" software (Qiagen) and build-in algorithms (core analysis) were used to identify regulators that are linked to the DEG in the two datasets. Note that the analysis were performed independently for both datasets to obtain unbiased lists of regulators that apply to the individual datasets. Interestingly, the software determined a ~60% overlap among the Top50 ranked regulators identified in both datasets (data not shown). The graph shows the regulators that are shared between both datasets and depicts the p-value by which they are linked to the two datasets (x-axis link to Supp.Fig. 1A dataset, y-axis link to Fig. 2E dataset). Highlighted in color are regulators with p-values of ≤ 10^{-8} in both datasets. **C**, total number of genes that are linked to the regulator in the Supp.Fig. 1A dataset (dysfunctional versus normal T cells) and the fraction that is controlled by Tox.

Supplementary Figure 6 - TOX deficient cells differentiate into functional memory T-cells during acute viral infection. A, $2x10^3$ CD45.1/2 ToxΔ^{Ex5} and CD45.1/1 wt P14 $CD8^+$ T-cells were transferred into C57BL/6 host mice which were then infected with $2x10^5$ PFU LCMV Armstrong. 1 or 4 weeks later, P14 cells were re-isolated, sorted by flow cytometry and either analyzed for gene expression profiles or transferred into secondary hosts. The secondary hosts were then infected with $2x10^5$ PFU LCMV Armstrong and analyzed on day 8 post infection. **B**,

RNA-sequencing analysis on day 8 after the primary LCMV Armstrong infection. The volcano plot shows data for all genes, yellow and green highlights genes with p-values ≤0.05 and Log_2 FC ≥ |0.5| and numbers indicate the genes that match the filter criteria. Heatmap showing differentially expressed genes (gene expression was transformed with Deseq2 (rlog) and then converted to z-score). **C**, shows representative dot plots of KLRG1, CD62L, and CD127 expression by ToxΔ^{Ex5} or wt P14 T-cells and corresponding frequencies in all mice at the time of transfer into the secondary hosts. **D**, Absolute numbers of Tcf-1^{+} ToxΔ^{Ex5} or wt P14 T-cells in the primary hosts at day 30 post infection as well as splenic expansion fold of ToxΔ^{Ex5} (light blue) and wt (dark bue) P14 T-cells in the secondary hosts 8 days after the re-challenge. Expansion was calculated assuming a 10% transfer efficacy.

Supplementary Figure 7 – Similar splenic localization of wt and ToxΔ^{Ex5} T-cells. C57BL/6 mice were engrafted with either ToxΔ^{Ex5} or wt P14 T-cells prior to infection with $5x10^6$ PFU LCMV clone-13. Spleens were harvested on day 8 (**A**) and day 14 (**B**) post infection and sections were stained with anti-B220 (blue), anti-CD3 (green), and anti-CD45.1 (red). Images of spleen sections were acquired with fluorescent microscope. The upper row shows representative microscopy of spleen sections. The whole section data were then vectorized using a density threshold-based algorithm to determine the red-pulp and the T-cell and the B-cell zone of the white pulp. The middle row shows examples of the vectorized data. Dark grey represents the B-cell zone, light grey the T-cell zone, and the clear background the red-pulp, red dots mark the location of individual P14 T-cells. The fraction of P14 T-cells in these three anatomical locations was then determined. The graphs on the bottom show the relative distribution of

wt P14 T-cells in 5 and of ToxΔ^{Ex5} P14 T-cells in 3 different hosts on day 8 (**A**) and wt P14 T-cells in 3 and ToxΔ^{Ex5} P14 T-cells in 4 different hosts on day 14 post infection (**B**).

Supplementary Figure 8 - Overexpression of TOX in human and mouse T-cells augments PD-1 expression, restricts cytokine production, and promotes acquisition of a dysfunctional phenotype. A, T-cells from healthy donors were ex-vivo activated by anti-CD3 and anti-CD28 stimulation and retrovirally transduced with human TOX gene. Untransduced T-cells serve as control. Representative histogram (top) and the percentage of PD-1 expressing cells (bottom). **B**, Similar as in A, TOX and TCR transduced T-cells [TOX group] or TCR-only transduced T-cells [Ctrl group] were co-cultured with SK-Mel-23 (grey) or 888-A2 (orange) cells for 16 hours and TNF and IFNγ production in the supernatant was measured using specific ELISAs. Baseline cytokine production following co-culture with antigen-negative T-cells was subtracted. Lines combine samples from the same donor with Tox or control overexpression. Paired t-tests comparing cytokine levels for all donors were performed with *<0.05; **p < 0.01; ns = not significant (p > 0.05). **C-F**, P14 T-cells transduced with 'empty-' or Tox-expressing retrovirus were transferred into Vβ5 host mice which were then infected with a mix of $0.5x10^6$ PFU LCMV wt clone-13 and $4.5x10^6$ gp-33 deficient clone-13. Splenocytes were collected 21 days post infection. **C**, fixed samples were co-analyzed for gfp expression and Tox. Gfp low and high gates were used to illustrate the direct correlation between transduction efficacy and Tox expression. **D**, Splenocytes were briefly *ex vivo* re-stimulated with gp33-peptide and stained intracellularly for cytokines. Shown are representative histograms and MFI data for TNF (left) and IFNγ (right) production by P14 T-cells. Tox overexpressing cells are depicted in light green and empty vector control in dark green. **E**, PD-1, KLRG1, and **F**, Tcf-1 expression levels in empty

vector (dark green) and Tox transduced P14s (light green). Symbols are data for individual mice; solid horizontal lines represent the mean. Unpaired t tests were performed with *<0.05; **p < 0.01; ns = not significant (p > 0.05).

Supplementary Figure 9 – Nr4a1 precedes Tox expression and induce TOX. A, naïve P14 TCR and Nur77 (Nr4a1) reporter transgenic T-cells were activated in vitro for 6 (left) and 24 hours (right) with anti-CD3/antiCD28 coated beads (top), with 0.1 ug/ml soluble anti-CD3 and 10ug/ml anti-CD28 (middle) antibody, or with 1 ug/ml anti-CD3 and 10ug/ml anti-CD28 (bottom) antibody. Cells were separated into Nr4a1 reporter positive (blue gates) and reporter negative gates (red gates). Shown are overlays of Tox expression levels in reporter positive and negative cells following bead stimulation (upper row) and reporter positive high and low dose anti-CD3 stimulated cells along with reporter negative cells as reference (middle row). **B**, naïve P14 TCR and Nur77 (Nr4a1) reporter transgenic T-cells were transferred into CD45 congenic C57BL/6 hosts. Mice were infected with LCMV $2x10^5$ PFU Armstrong, $5x10^6$ PFU wt LCMV clone-13, or $0.5x10^6$ PFU wt clone-13 mixed with 4.5 $x10^6$ PFU gp33-deficient LCMV clone-13 mutant strain. P14 were isolated on day 10 post infection and analyzed for Tox along with Nur77 reporter expression. **C**, Isolated $CD8^+$ T-cells were in vitro activated with anti-CD3/anti-CD28 beads for 24h and then retrovirally transduced with Tox, Nr4a1, Ifr4 or empty control vectors. 4 days later intracellular staining for Tox was performed. Representative histograms (left) of Tox expression and Tox MFI data (right) are shown. **D**, the Gene Transcription Regulation Database (GTRD, *http://gtrd.biouml.org/*) was used to extract from all deposited data transcription factors (TF), which bind to the TOX locus and binding to the Tox gene is illustrated for Batf, Irf4, and Nr4a1. **E**, Putative upstream located transcription

factors (Bold italic) of Tox were retrived from the "Ingenuity pathway analysis" database. The networks shows all genes, for which the database has upstream connections with the transcription factors, and which are included in the DEG list defined by AverageExpression >6, $p<0.05$, and Log_2 FC ≥ |0.3| for the Supp.Fig. 1A dataset (normal versus dysfunctional T cells). Green symbols indicated decreased and red symbols increased expression in the dataset. Symbols in blue and orange color (only for NKX2-1) indicate predicted activity that is based expression activity in the connected genes and the type of connection. Color intensity grading indicate the level of differential expression or the level of predicted activity. Arrow color coding indicate the match between gene expression data and information retrieved for these connections from the database. Note that a connection between Nr4a1 and Tox was not included in the database but given the induction of Tox following Nr4a1 overexpression (shown in C), it was manually added by us to the network. Connections to genes from the DEG list were established as for the other transcription factors.

Supplementary Figure 10 - TOX deletion enhances T-cell effector function, and exacerbates T-cell mediated immunopathology. Lung (**A**) and liver (**B**) pathology in C57BL/6 mice (n = 5) given $1x10^4$ ToxΔ^{Ex5} or wt P14 T-cells as described in Fig. 2 prior to infection with $5x10^6$ PFU LCMV clone-13. Host mice were assessed 11 days later. Scale bar, 50 µm**.** Blue doted lines mark the periportal regions with large cellular infiltrates in wt p14 recipients while the green dotted lines highlight necrotic zones that are found only in mice which received ToxΔ^{Ex5} T-cells. **C**, shown are quantitative assessments of semiquantitative (lung pathology) scoring and liver necrosis (Ishak Score).

Supplementary Figure 11 – Tox deficiency impacts phenotype and maintenance of both high and low affinity T-cells but not proliferation activity. C57BL/6 mice are engrafted with either ToxΔ^{Ex5} or wt P14 T-cells obtained from PolyIC treated donor mice as explained in Fig. 2. Mice were then infected with 5x10^6 PFU wt LCMV clone-13 (high affinity) or the altered peptide ligand (APL) encoding C6 variant of clone-13 (low affinity[2]). Blood was collected on day 7 and 13 post infection. **A**, ratio of ToxΔ^{Ex5} and wt T-cells on day 7 and 13 post infection. **B**, representative histograms and MFI data for PD-1 (top) and KLRG1 (bottom) at the indicated time-points with dark color coding for wt p14 and light color for ToxΔ^{Ex5} P14 as well as blue color for normal and red color for the C6 APL clone-13 variant. **C**, C57BL/6 mice are engrafted with ToxΔ^{Ex5} or wt P14 T-cells obtained from PolyIC treated donor mice. Host mice were infection with 5x10^6 PFU LCMV clone-13. On day 13 post infection, 1 mg of EdU was injected I.P. and spleens were collected 6 hours later. Representative flow cytometry plots of EdU^+ incorporation into P14 T-cells and percentage of EdU^+ ToxΔ^{Ex5} (light blue) or wt (dark blue) P14 T-cells. Unpaired t tests were performed with *<0.05; **p < 0.01; ns = not significant (p > 0.05).

Supplementary Figure 12 – Pathway activity analysis for the Tim3- population. A DEG list defined by MeanExpression >50, p<0.05, and Log_2 FC ≥ |0.5| was determined for $Tim3^+$ ToxΔ^{Ex5} versus $Tim3^+$ wt P14 T cells. The Data were submitted to "Ingenuity pathway analysis - core analysis". Depicted in decreasing order are the Top pathways determined by the software. Details are shown for the "cellular growth and proliferation pathway" and "cell death and survival". Orange color indicated heighted activity and blue lower activit for ToxΔ^{Ex5} versus versus wt P14 T cells.

Supplementary Figure 13 –Tox promotes genome-wide DNA methylation reprogramming. C57BL/6 mice engrafted with wt or ToxΔ^{Ex5} 2x10^3 P14 T-cells were infected with 2x10^6 PFU clone-13. On day 8 post infection, splenic wt and ToxΔ^{Ex5} P14 T-cells were sorted into Tim-3^+ and Tim-3^- T-cells and whole-genome DNA methylation analysis was performed. **A**, Heatmap showing cluster analysis of the top 3,000 differentially methylated regions (DMRs) between ToxΔ^{Ex5} and wt P14 T-cells. Color intensity scales from red (methylated region) to blue (non-methylated region). **B**, absolute number of DMRs between Tox$\Delta^{Ex5}$and wt P14 T-cells on Tim3^+ (left, red) or Tim3^- (green, right) population. **C**, Venn diagram show the absolute number of overlapping DMRs that are more methylated in P14 ToxΔ^{Ex5} and in naive P14 T-cells relative to wt P14 on day 8 post infection for the Tim3^+ (left) or Tim3^- (right) population. **D**, Correlation analysis of differentially methylated regions (DMR) and differentially expressed genes (DGE) on day 8 post infection for Tim3^+ ToxΔ^{Ex5} and wt P14 T-cells (left) and for Tim3^- ToxΔ^{Ex5} and wt P14 T-cells (right). The DMR values are then plottet against matching data from the differential gene exrpession analysis shown in Figure 4. **E)** Bar graph showing NCI-Nature 2016 pathways that are significantly enriched among genes undergoing DNA demethylation (> 20% change in DNA methylation frequency) in the Tim3^+, or **(F)** Tim3^- subsets of WT *versus* ToxΔ^{Ex5} antigen-specific CD8 T cells isolated on day 8 after chronic LCMV infection.

Supplementary Figure 14 - Global and locus specific accessibility difference in the absence of Tox. C57BL/6 mice are engrafted with either ToxΔ^{Ex5} or wt P14 T-cells prior to infection with 5x10^6 PFU LCMV clone-13. Splenocytes are collected on day 8 and 13 post infection and Atac-sequencing was performed as indicated in the methods section. **A**, Bar graph summarizing the numbers of differentially open chromatin regions (*OCRs) among ToxΔ^{Ex5} versus wt P14 T-

cells on day 8 (left) and 13 (right) post infection. **B,** Genome browser snapshots of Atac-seq peak intensity in the Pdcd1 (top) and TNF (bottom) locus for ToxΔ^{Ex5} (pink) or wt P14 T-cells (black). Notable differences in chromatin accessibility are highlighted by red boxes. *OCR is defined as a genomic region with differential chromatin accessibility of $Log_2FC \geq 2$ and adjusted p-value ≤ 0.05 as a cutoff. **C)** Bar graph showing Biocarta pathways that are significantly enriched among genes with ATAC-seq peaks that gained (green), or **(D)** lost (red) chromatin accessibility ($Log_2FC \geq 1$) in ToxΔ^{Ex5} *versus* WT antigen-specific CD8 T cells isolated on day 13 after chronic LCMV infection.

Supplementary Figure 15 – Transcriptional network connections for Tox controlled T cell dysfunction associated genes. A, Venn diagram similar to Supp.Fig. 5A but showing only the number of DEG for dysfunctional versus no dysfunctional P14 T cells (Supp.Fig. 1A) and wt versus ToxΔ^{Ex5} (Fig. 2E). **B**. The overlapping 269 DEG from A were imported into "Ingenuity pathway analysis" and a core analysis" was performed. Depicted are the p-values for the associated upstream transcription factors or transcription regulators (jointly referred to as TR) plus the number of genes linked to these molecules. The Top regulators are annotated and molecules of interest are highlighted in color. **C**, Connections of DEG to selected TR, green symbols indicated decreased and red symbols increased expression in dysfunctional versus non dysfunctional P14 T cells (Supp.Fig 1A dataset), purple indicates connections to TR differentially expressed in the Supp.Fig. 1A dataset. **D**, shows "Ingenuity pathway analysis" determined connections among the Top regulators (p-value $<10^{-5}$). Colors indicate differential gene expression (as explained in C) within the datasets shown in Fig. 4E. The left plot shows

wt versus ToxΔ^{Ex5} P14 T cells in the Tim3^{+} population and the right plot similar data for Tim3^{-} cells.

Supplementary Figure 16 – Proposed dynamics of wild-type and Tox deficient antigen-specific T-cell populations in chronic infection. We consider that an initial wave of effector committed T-cells acquire some signs of dysfunction independently of Tox. Yet, absence of Tox results in a failure to epigenetically enforce a dysfunctional phenotype in the critical Tcf-1 expressing (Tim-3 negative) memory-like population. The over-time increasing phenotypic changes at the level of the entire population are then the consequence of the continuous replacement of the effector committed Tcf-1 negative T-cells from the improperly programmed Tcf-1 positive population. This processes happen in parallel to the decline of the total population caused by declining absolute numbers of Tcf-1 positive T-cells in the absence of Tox.

References:

1 Cornberg, M. *et al.* Clonal exhaustion as a mechanism to protect against severe immunopathology and death from an overwhelming CD8 T cell response. *Frontiers in immunology* **4**, 475, doi:10.3389/fimmu.2013.00475 (2013).

2 Utzschneider, D. T. *et al.* High antigen levels induce an exhausted phenotype in a chronic infection without impairing T cell expansion and survival. *The Journal of experimental medicine* **213**, 1819-1834, doi:10.1084/jem.20150598 (2016).

Figure 1

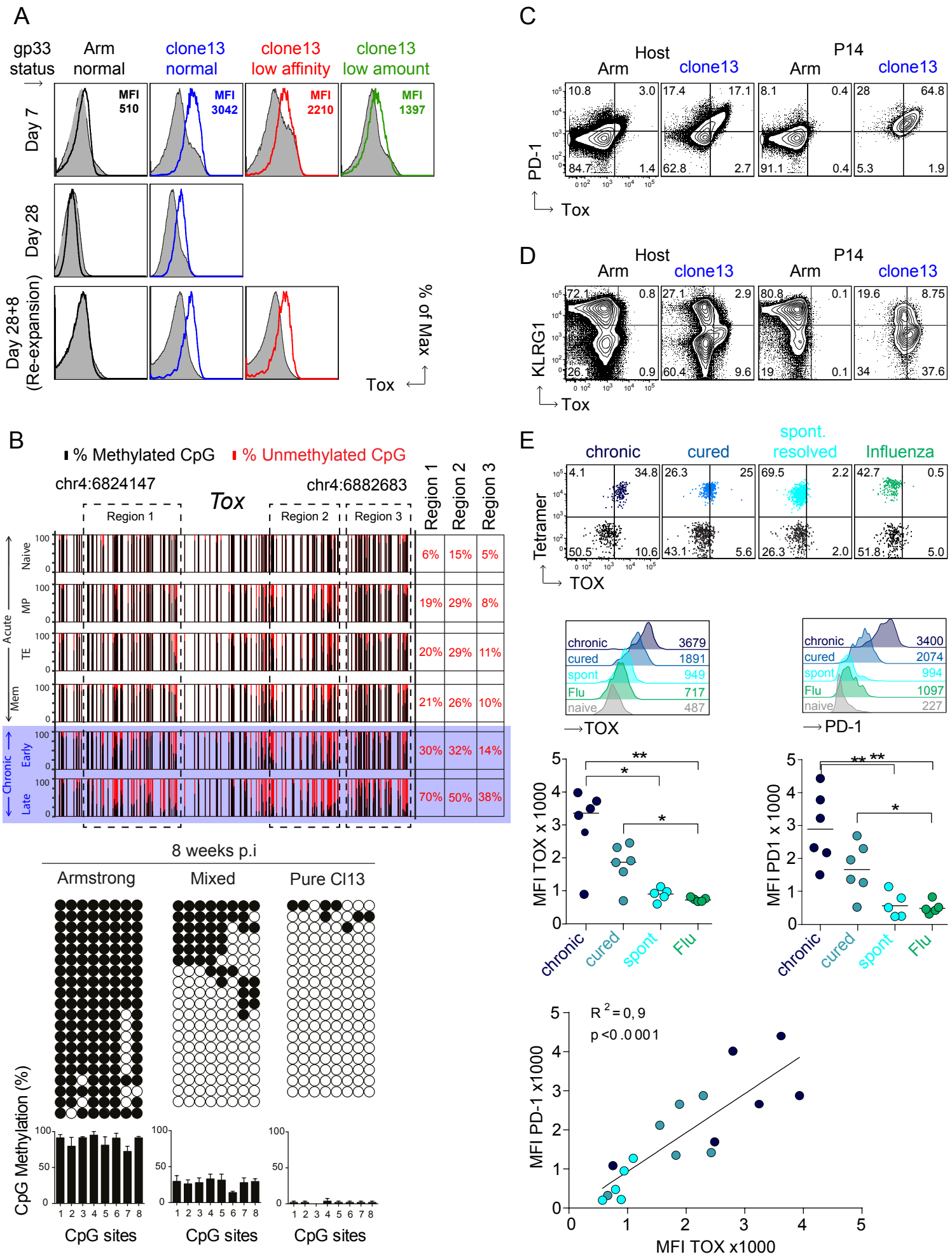
A
gp33 status
Arm normal
clone13 normal
clone13 low affinity
clone13 low amount
Day 7
Day 28
Day 28+8 (Re-expansion)
MFI 510
MFI 3042
MFI 2210
MFI 1397
% of Max
Tox
B
% Methylated CpG
% Unmethylated CpG
chr4:6824147
chr4:6882683
Tox
Region 1
Region 2
Region 3
Naive
MP
TE
Mem
Acute
Chronic
Early
Late
6% 15% 5%
19% 29% 8%
20% 29% 11%
21% 26% 10%
30% 32% 14%
70% 50% 38%
8 weeks p.i
Armstrong
Mixed
Pure Cl13
CpG Methylation (%)
CpG sites
C
Host
P14
Arm
clone13
PD-1
Tox
10.8 3.0 84.7 1.4
17.4 17.1 62.8 2.7
8.1 0.4 91.1 0.4
28 64.8 5.3 1.9
D
KLRG1
72.1 0.8 26.1 0.9
27.1 2.9 60.4 9.6
80.8 0.1 19 0.1
19.6 8.75 34 37.6
E
chronic
cured
spont. resolved
Influenza
Tetramer
TOX
4.1 34.8 50.5 10.6
26.3 25 43.1 5.6
69.5 2.2 26.3 2.0
42.7 0.5 51.8 5.0
chronic 3679
cured 1891
spont 949
Flu 717
naive 487
chronic 3400
cured 2074
spont 994
Flu 1097
naive 227
PD-1
MFI TOX x 1000
MFI PD1 x 1000
R 2 = 0, 9
p <0 .0 001
MFI PD-1 x1000
MFI TOX x1000

Figure 2

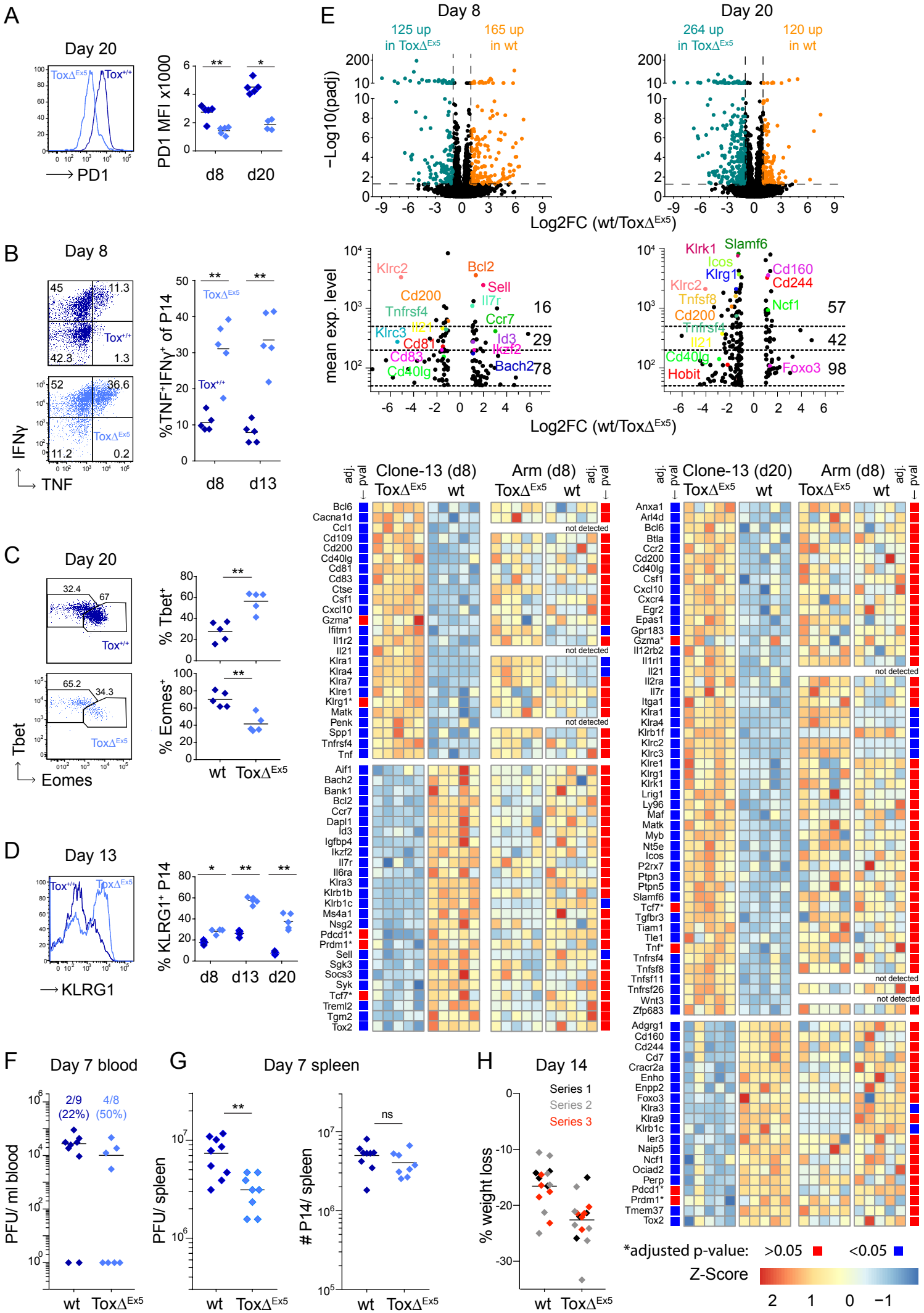
A
Day 20
ToxΔEx5
Tox+/+
PD1
PD1 MFI x1000
d8
d20
B
Day 8
IFNγ
TNF
%TNF+IFNγ+ of P14
d8
d13
C
Day 20
Tbet
Eomes
% Tbet+
% Eomes+
wt
ToxΔEx5
D
Day 13
KLRG1
% KLRG1+ P14
d8
d13
d20
E
Day 8
Day 20
125 up in ToxΔEx5
165 up in wt
264 up in ToxΔEx5
120 up in wt
−Log10(padj)
Log2FC (wt/ToxΔEx5)
mean exp. level
Klrc2
Bcl2
Sell
Cd200
Il7r
Tnfrsf4
Ccr7
Klrc3
Il21
Cd81
Id3
Cd83
Ikzf2
Cd40lg
Bach2
Klrk1
Slamf6
Icos
Klrg1
Cd160
Cd244
Tnfsf8
Ncf1
Hobit
Foxo3
Clone-13 (d8)
Arm (d8)
Clone-13 (d20)
adj. pval
not detected
F
Day 7 blood
2/9 (22%)
4/8 (50%)
PFU/ ml blood
G
Day 7 spleen
PFU/ spleen
P14/ spleen
ns
H
Day 14
Series 1
Series 2
Series 3
% weight loss
*adjusted p-value: >0.05 <0.05
Z-Score
2 1 0 −1

Figure 3

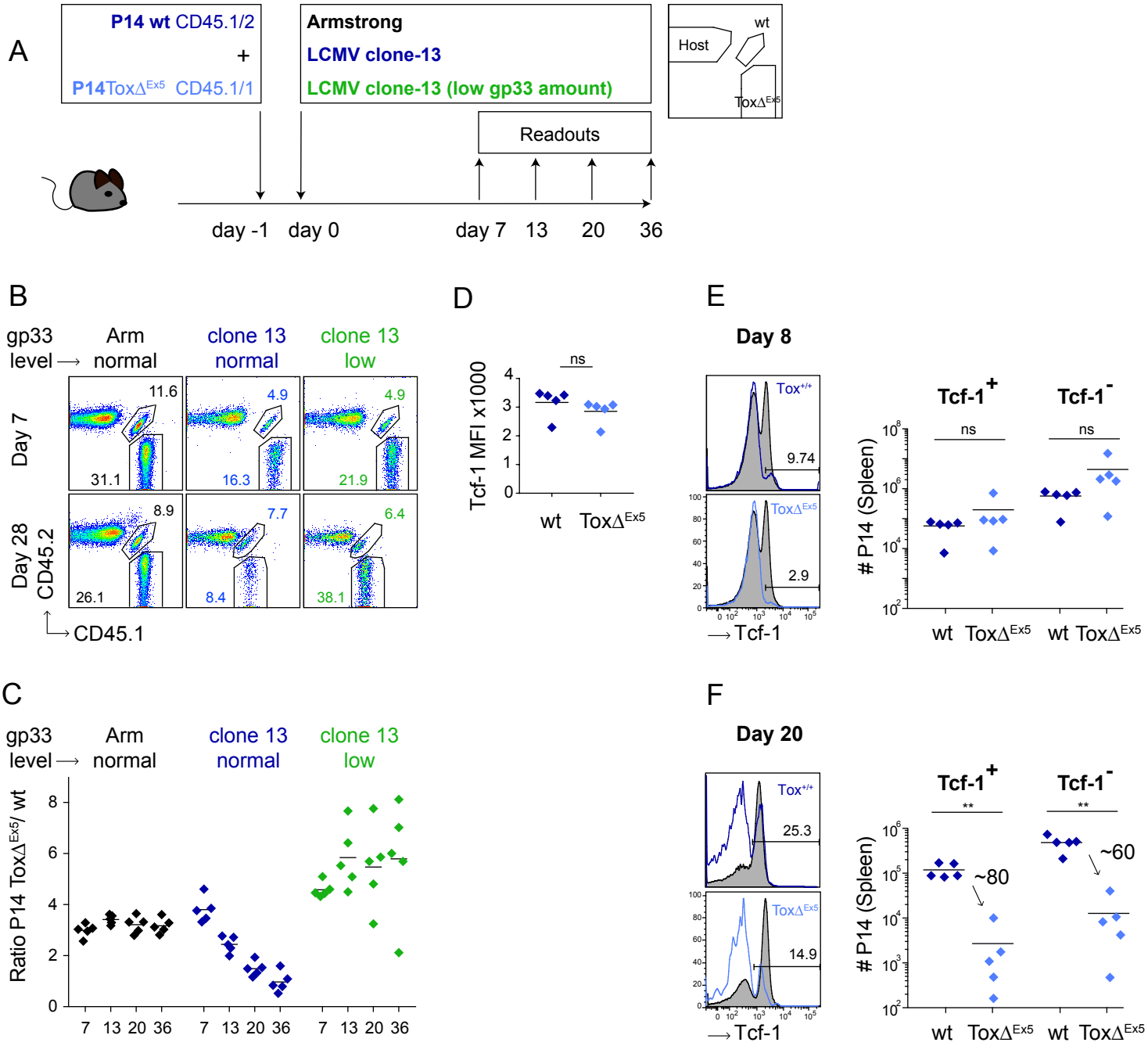
A
P14 wt CD45.1/2
+
P14ToxΔEx5 CD45.1/1
Armstrong
LCMV clone-13
LCMV clone-13 (low gp33 amount)
Readouts
Host
wt
ToxΔEx5
day -1
day 0
day 7
13
20
36
B
gp33 level
Arm normal
clone 13 normal
clone 13 low
Day 7
Day 28
CD45.2
CD45.1
11.6
31.1
4.9
16.3
4.9
21.9
8.9
26.1
7.7
8.4
6.4
38.1
C
Ratio P14 ToxΔEx5/ wt
D
Tcf-1 MFI x1000
ns
wt
ToxΔEx5
E
Day 8
Tox+/+
9.74
ToxΔEx5
2.9
Tcf-1
Tcf-1+
Tcf-1-
P14 (Spleen)
F
Day 20
25.3
14.9
~80
~60
**

Figure 4

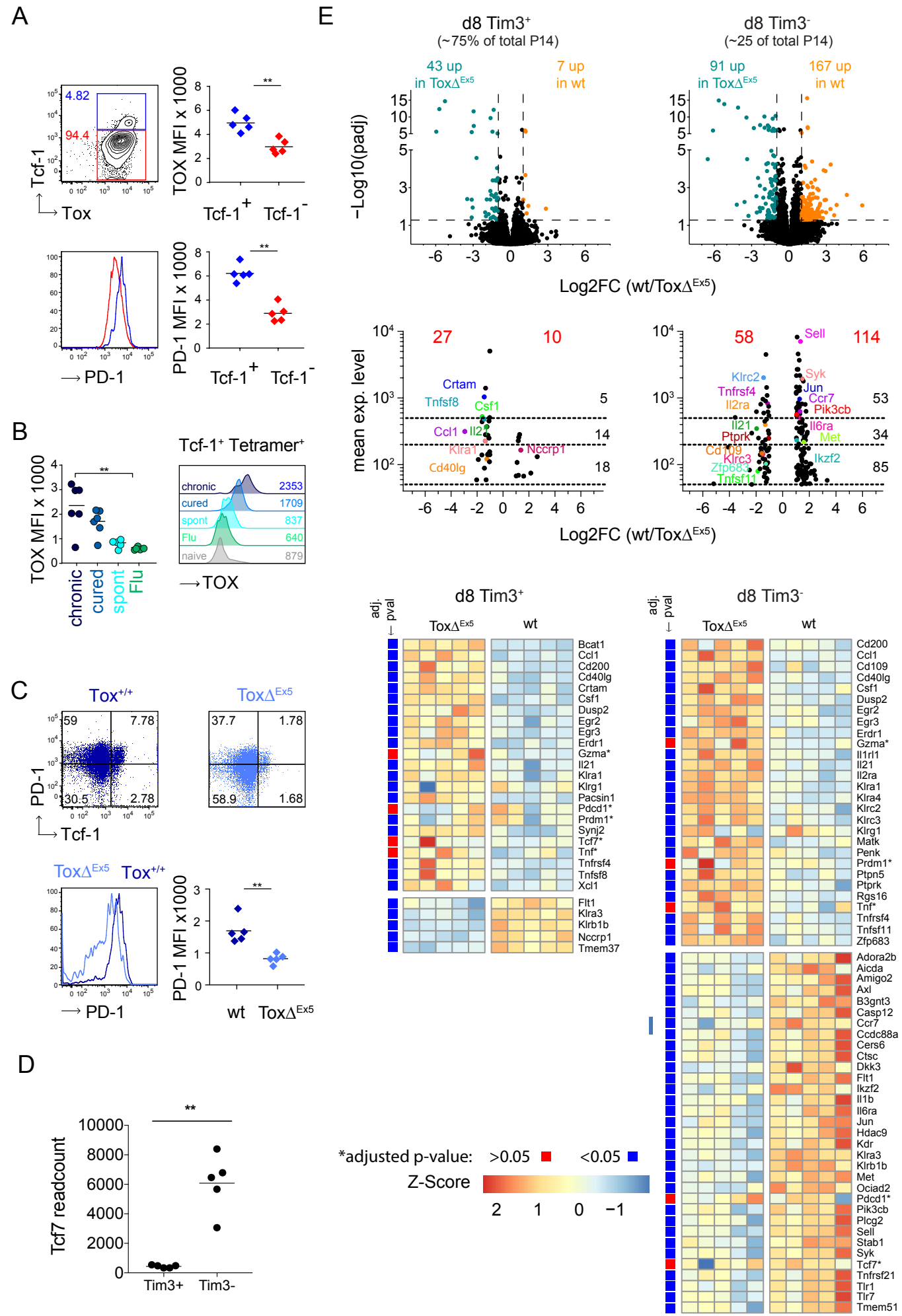
A
4.82
94.4
Tcf-1
Tox
TOX MFI x 1000
Tcf-1+
Tcf-1-
PD-1
PD-1 MFI x 1000
B
Tcf-1+ Tetramer+
TOX MFI x 1000
chronic
cured
spont
Flu
2353
1709
837
640
879
naive
TOX
C
Tox+/+
ToxΔEx5
59
7.78
30.5
2.78
37.7
1.78
58.9
1.68
PD-1
Tcf-1
PD-1 MFI x1000
wt
D
Tcf7 readcount
Tim3+
Tim3-
E
d8 Tim3+
(~75% of total P14)
43 up in ToxΔEx5
7 up in wt
d8 Tim3-
(~25 of total P14)
91 up in ToxΔEx5
167 up in wt
−Log10(padj)
Log2FC (wt/ToxΔEx5)
mean exp. level
27
10
5
14
18
58
114
53
34
85
Crtam
Tnfsf8
Csf1
Ccl1
Il2
Klra1
Nccrp1
Cd40lg
Sell
Klrc2
Syk
Tnfrsf4
Jun
Il2ra
Ccr7
Pik3cb
Il21
Il6ra
Ptprk
Met
Cd109
Klrc3
Ikzf2
Zfp683
Tnfsf11
adj. pval
ToxΔEx5
wt
Bcat1
Ccl1
Cd200
Cd40lg
Crtam
Csf1
Dusp2
Egr2
Egr3
Erdr1
Gzma*
Il21
Klra1
Klrg1
Pacsin1
Pdcd1*
Prdm1*
Synj2
Tcf7*
Tnf*
Tnfrsf4
Tnfsf8
Xcl1
Flt1
Klra3
Klrb1b
Nccrp1
Tmem37
Cd200
Ccl1
Cd109
Cd40lg
Csf1
Dusp2
Egr2
Egr3
Erdr1
Gzma*
Il1rl1
Il21
Il2ra
Klra1
Klra4
Klrc2
Klrc3
Klrg1
Matk
Penk
Prdm1*
Ptpn5
Ptprk
Rgs16
Tnf*
Tnfrsf4
Tnfsf11
Zfp683
Adora2b
Aicda
Amigo2
Axl
B3gnt3
Casp12
Ccr7
Ccdc88a
Cers6
Ctsc
Dkk3
Flt1
Ikzf2
Il1b
Il6ra
Jun
Hdac9
Kdr
Klra3
Klrb1b
Met
Ociad2
Pdcd1*
Pik3cb
Plcg2
Sell
Stab1
Syk
Tcf7*
Tnfrsf21
Tlr1
Tlr7
Tmem51
*adjusted p-value: >0.05 <0.05
Z-Score
2 1 0 −1

Supplementary figure 1

A

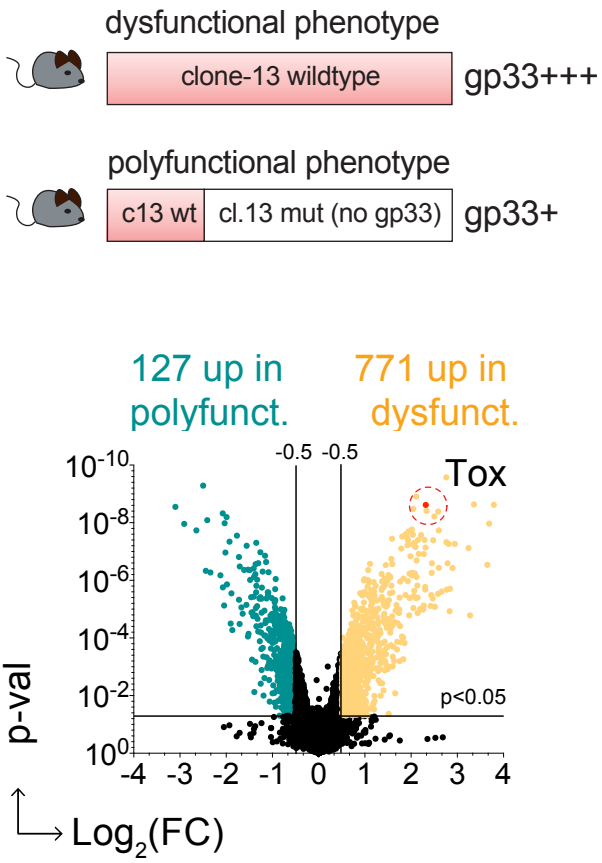

Signature genes of dysfunctional cells (FC>2), p<0.05

GeneName	Log_2(FC)	GeneName	Log_2(FC)
Pkdcc	4.74	Osgin1	2.47
Penk	3.79	Nr4a2	2.45
Ccr6	3.69	Slamf6	2.45
Xcl1	3.65	Zbtb32	2.34
Lag3	3.36	Tox	2.32
Id3	3.24	Tacc2	2.31
Perp	2.90	Drc1	2.31
Cxcl10	2.84	Hist1h2ab	2.31
Tnfsf8	2.83	Cd9	2.17
Rgs16	2.79	Myb	2.14
Cxcr5	2.77	Hist2h3b	2.14
Tigit	2.76	Itgad	2.12
Gpr56	2.64	Sema7a	2.10
Hist1h1b	2.60	Socs3	2.06
Cables1	2.60	Pglyrp1	2.04
Ier5l	2.51	Rgs10	2.03
Pdcd1	2.50	Jdp2	2.02
Enho	2.48	Dusp6	2.02

GeneName	Log_2(FC)
Stx1a	-2.03
Fcgr2b	-2.07
Klrg1	-2.41
Esm1	-2.44
Gpr114	-2.50
Kcnj8	-2.50
Gpr97	-2.60
Prss12	-2.91

B

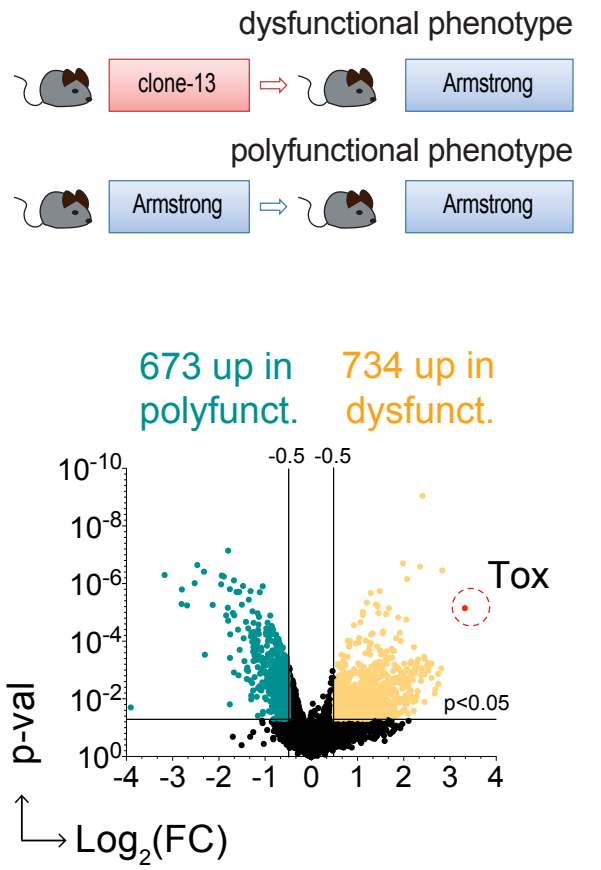

C

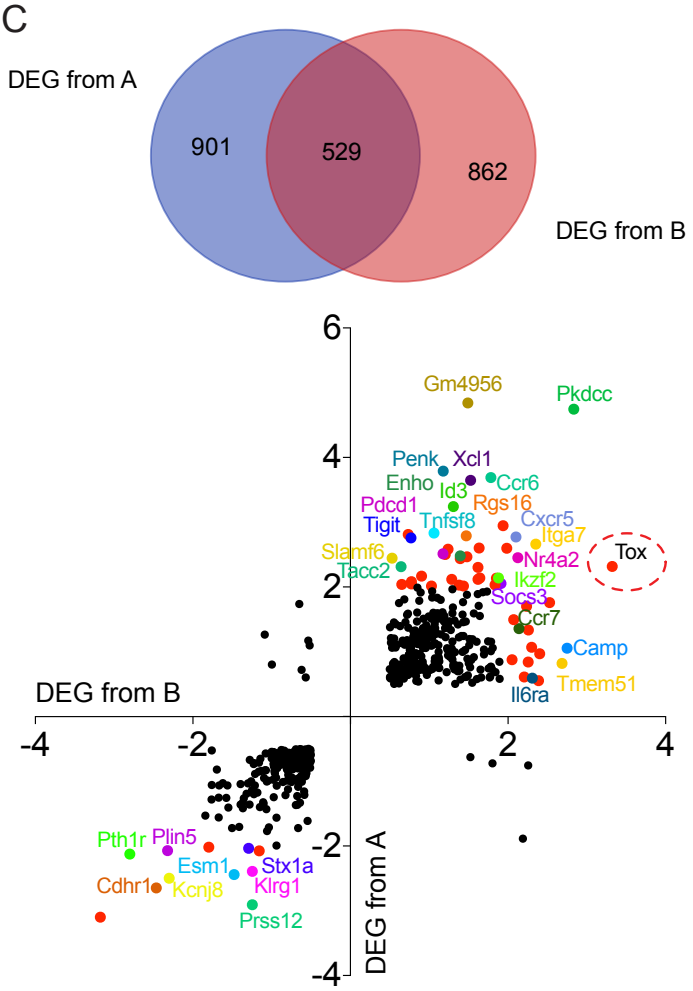

Supplementary Figure 2

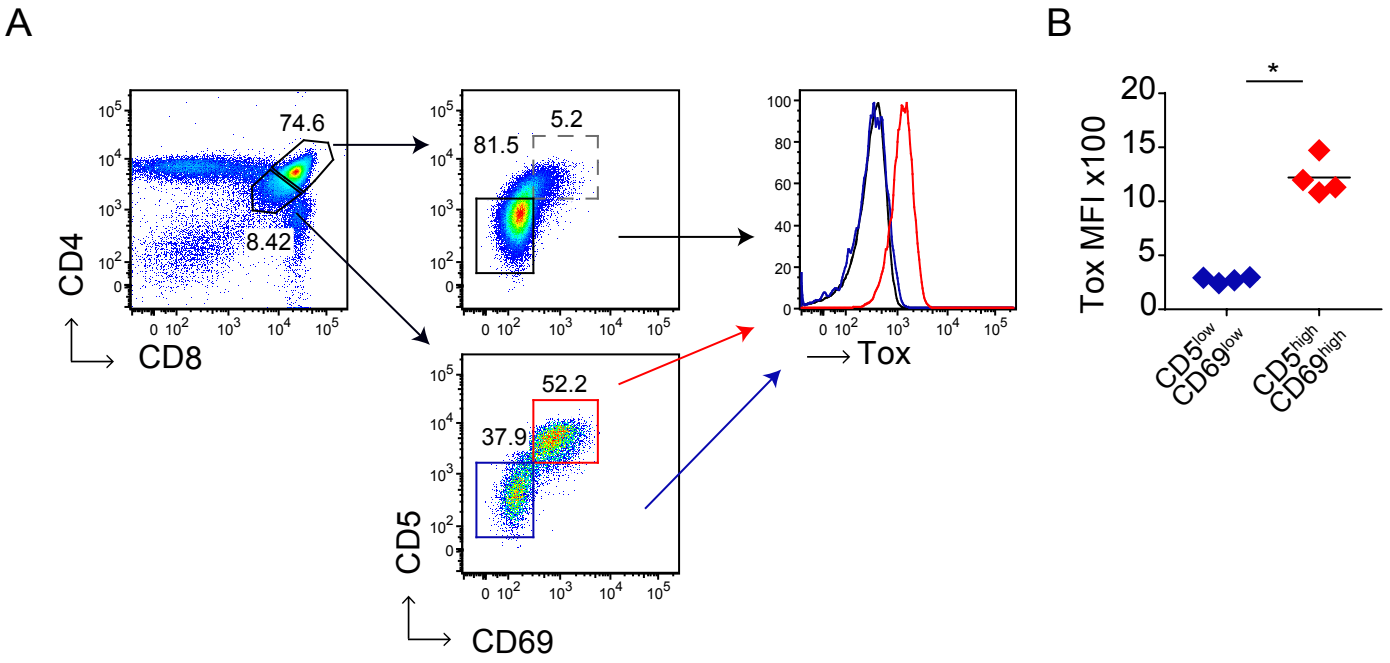

Supplementary Figure 3

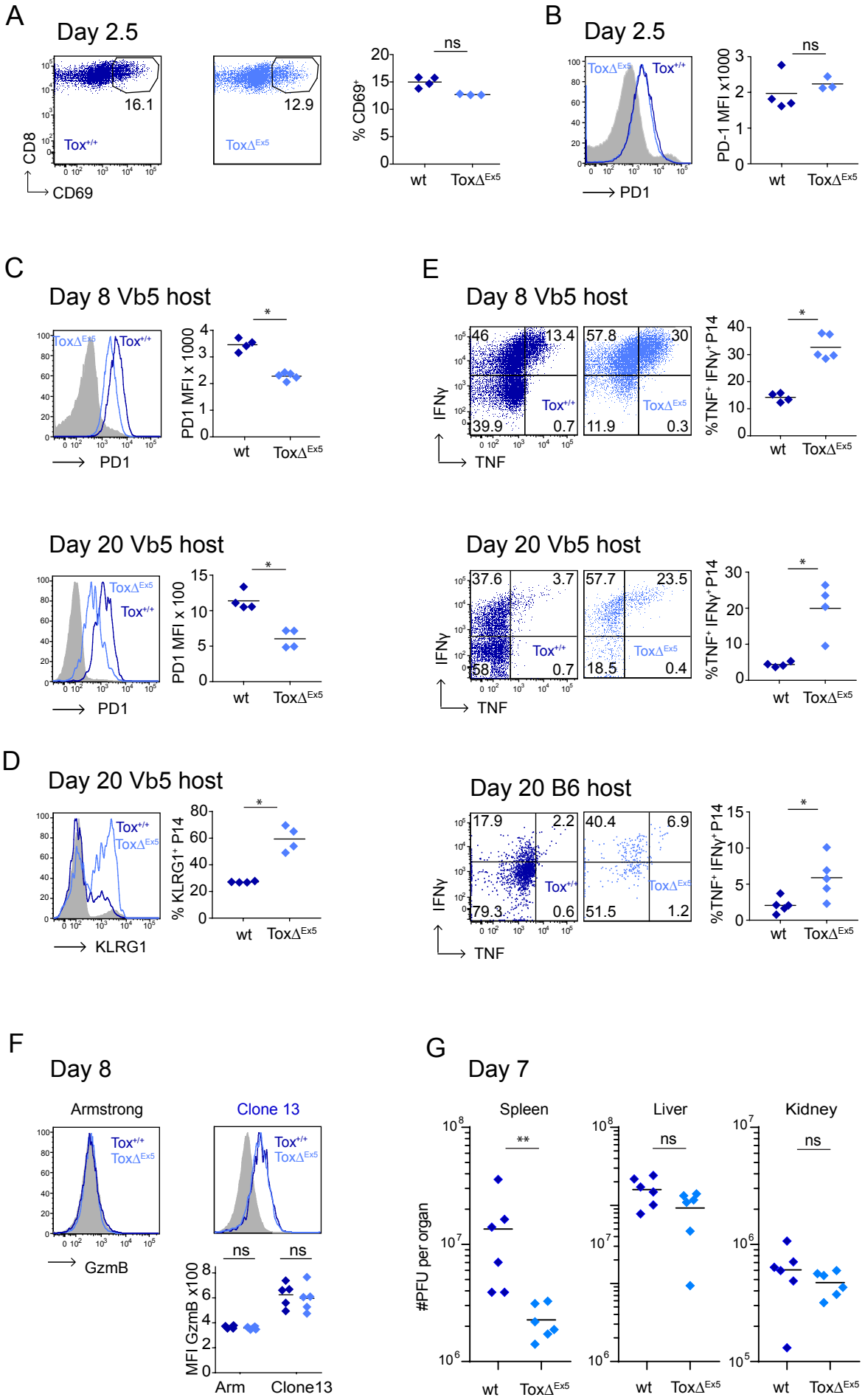

Supplementary Figure 4

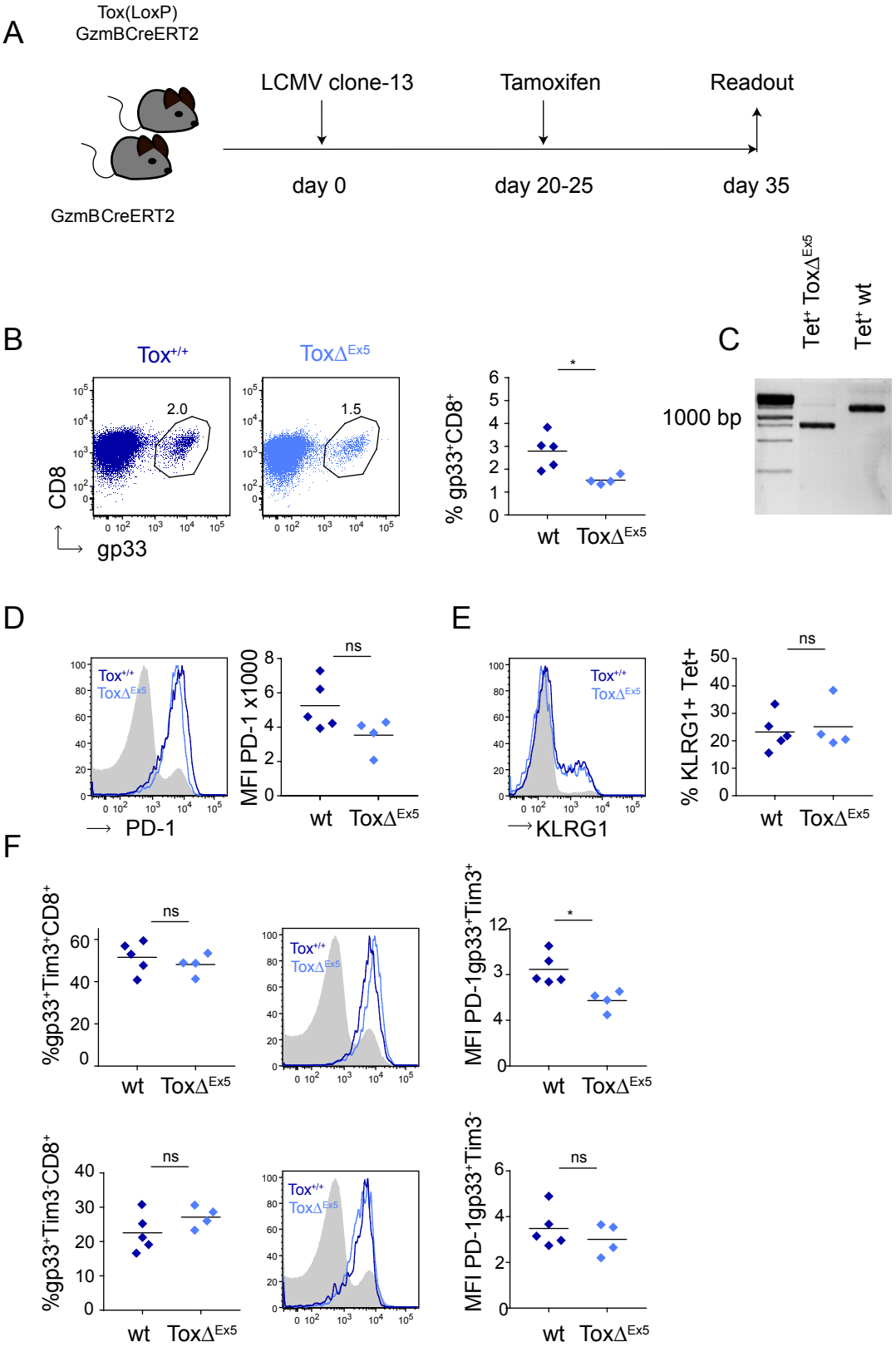

Supplementary Figure 5

A

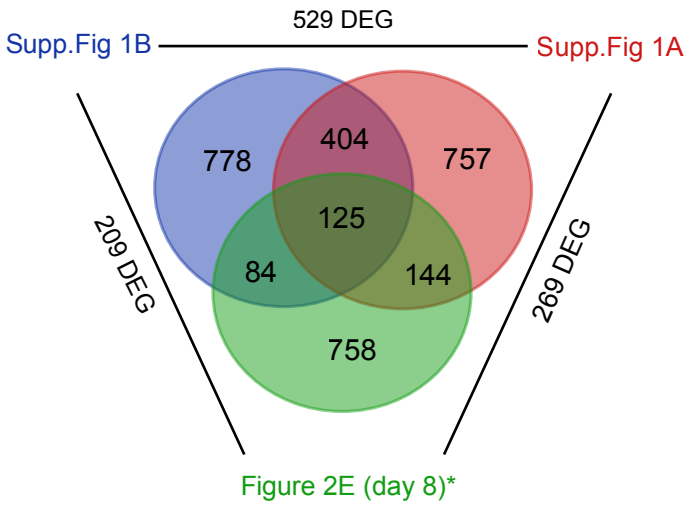

*note: a lower thereshold than in figure 2E was applied to facilitate IPA analysis, which resulted in a larger DEG list.

B

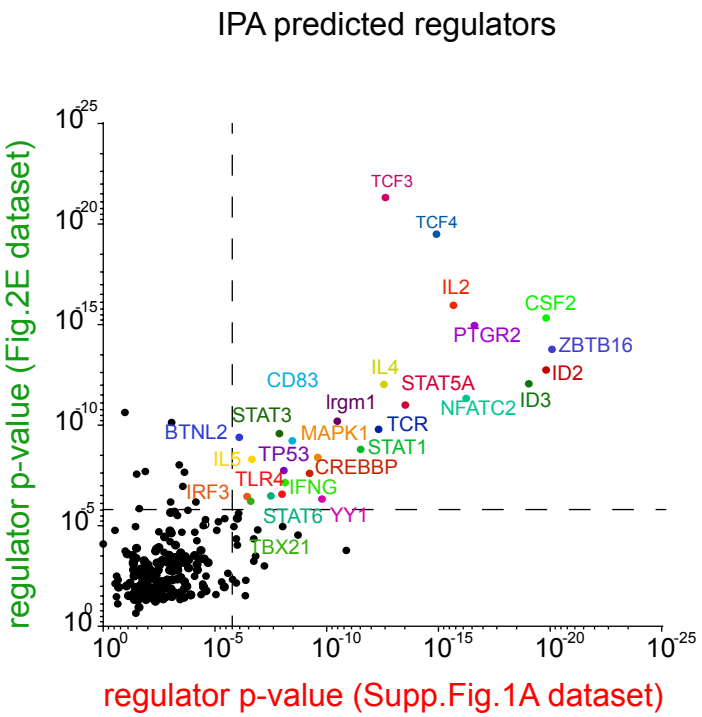

C

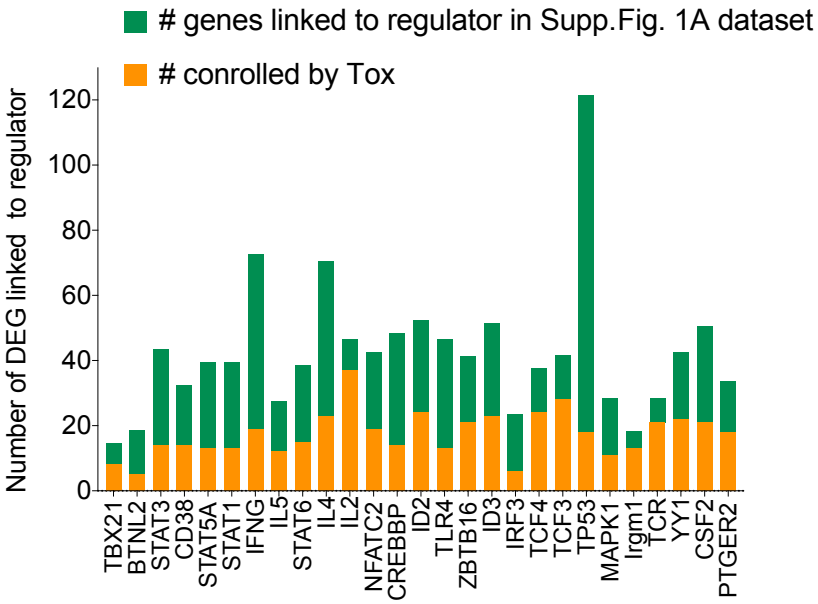

Supplementary Figure 6

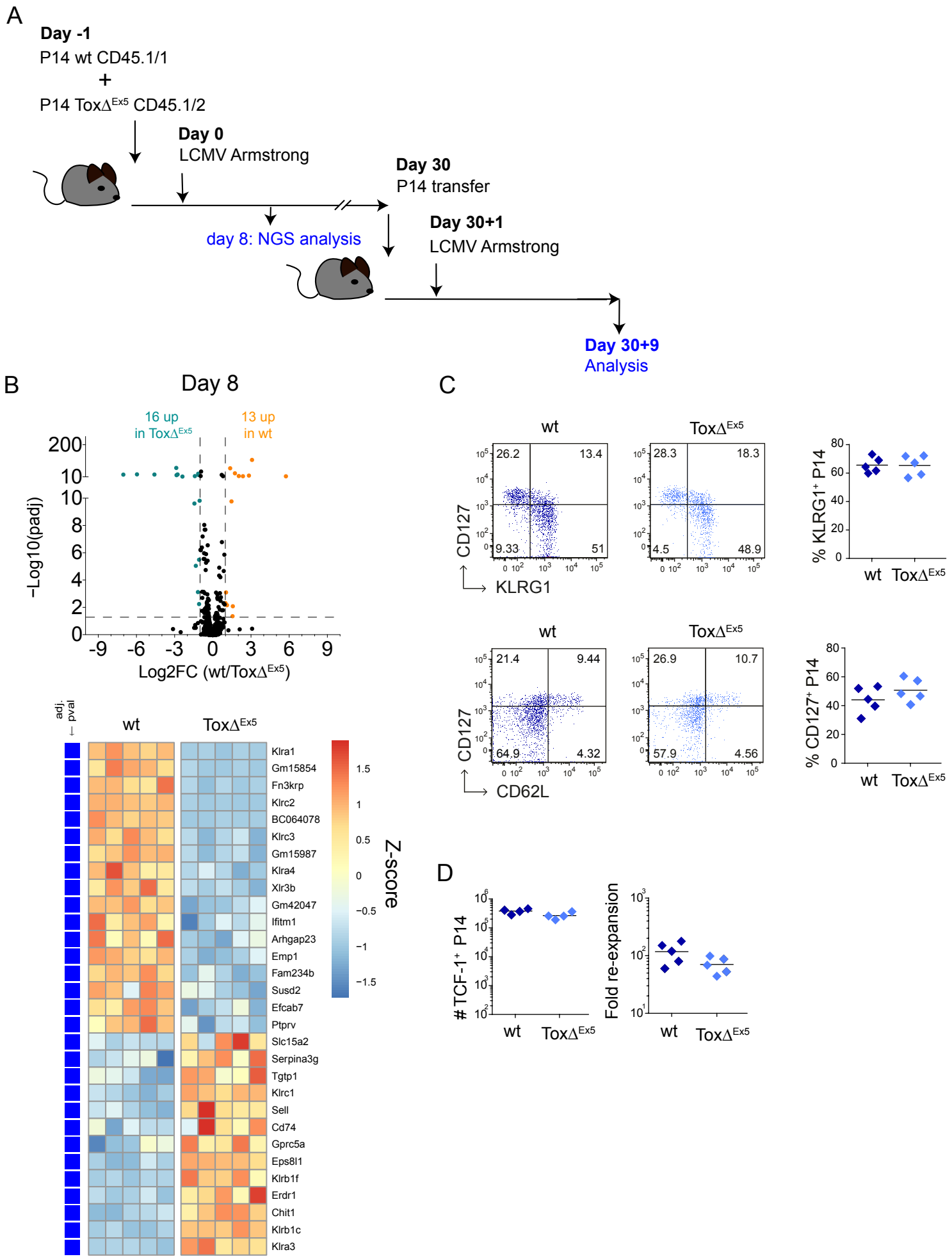

Supplementary Figure 7

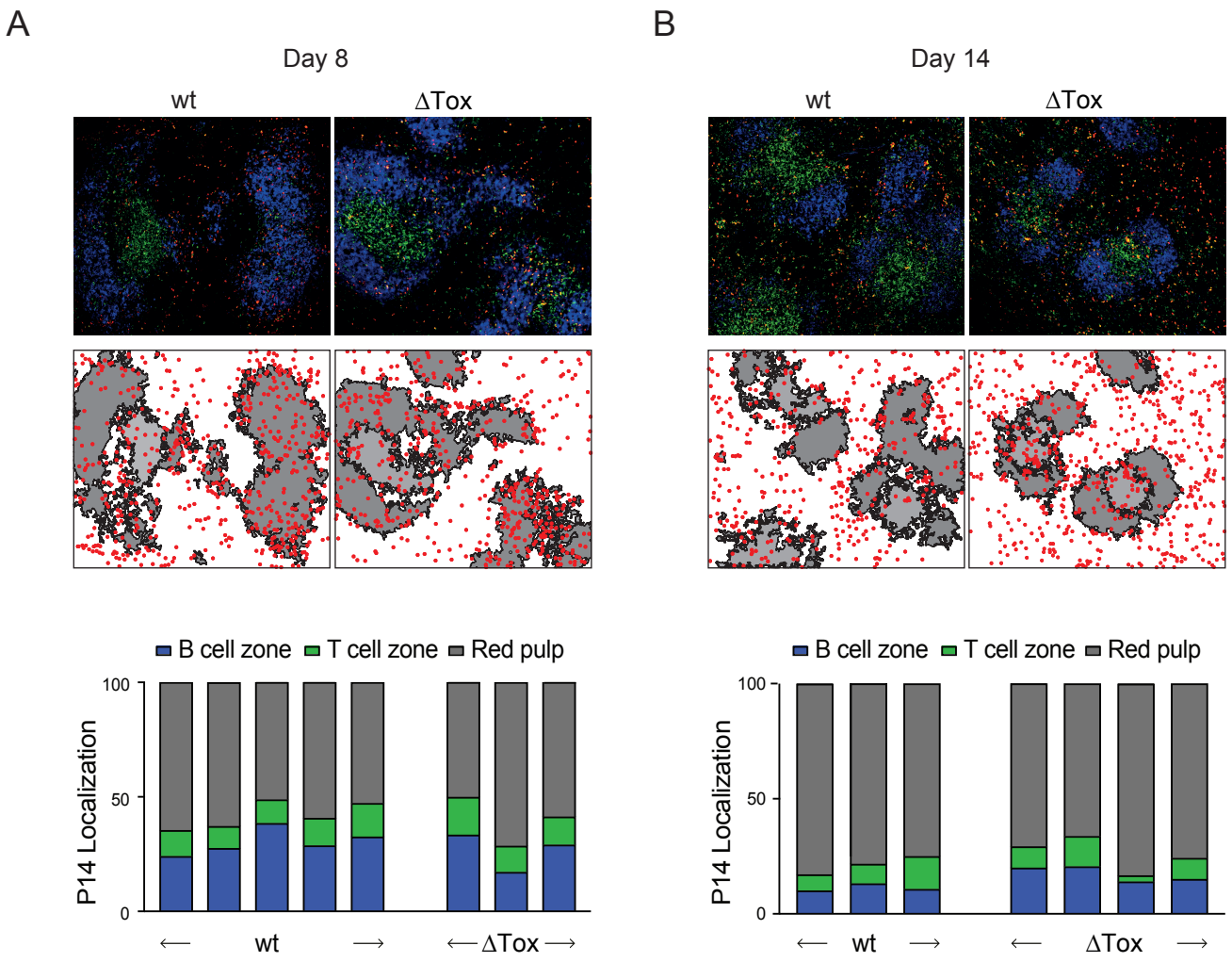

Supplementary Figure 8

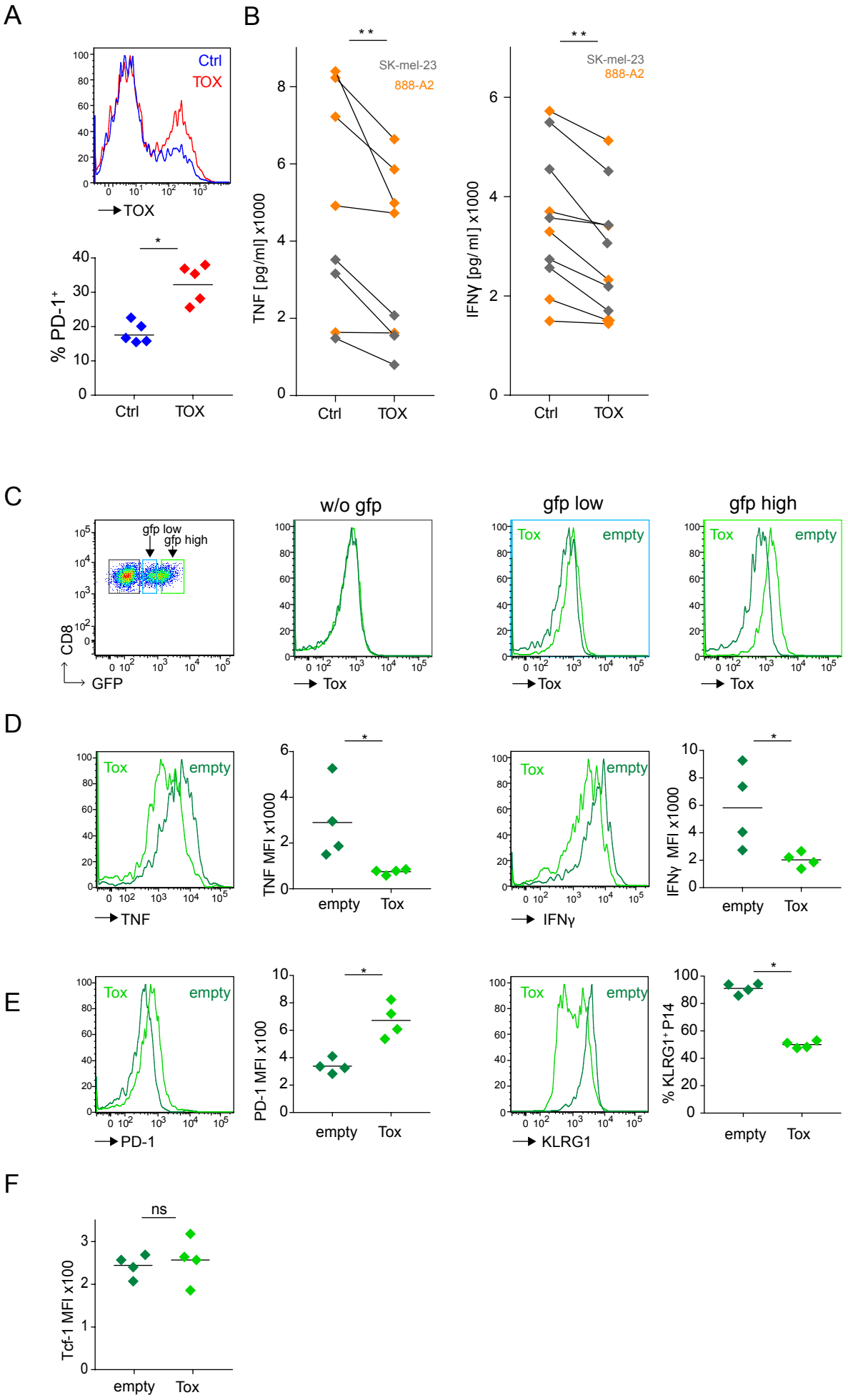

Supplementary Figure 9

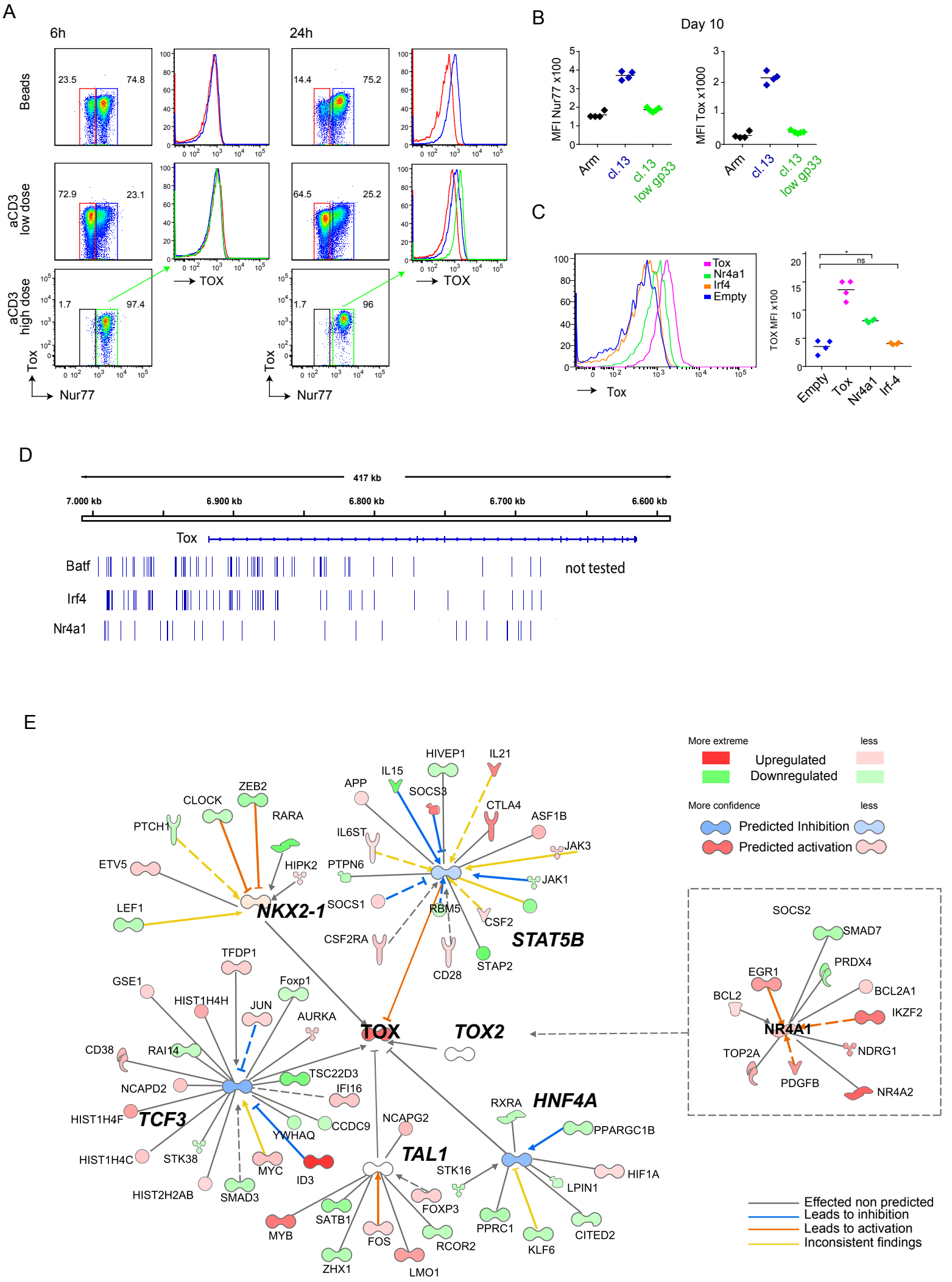

Supplementary Figure 10

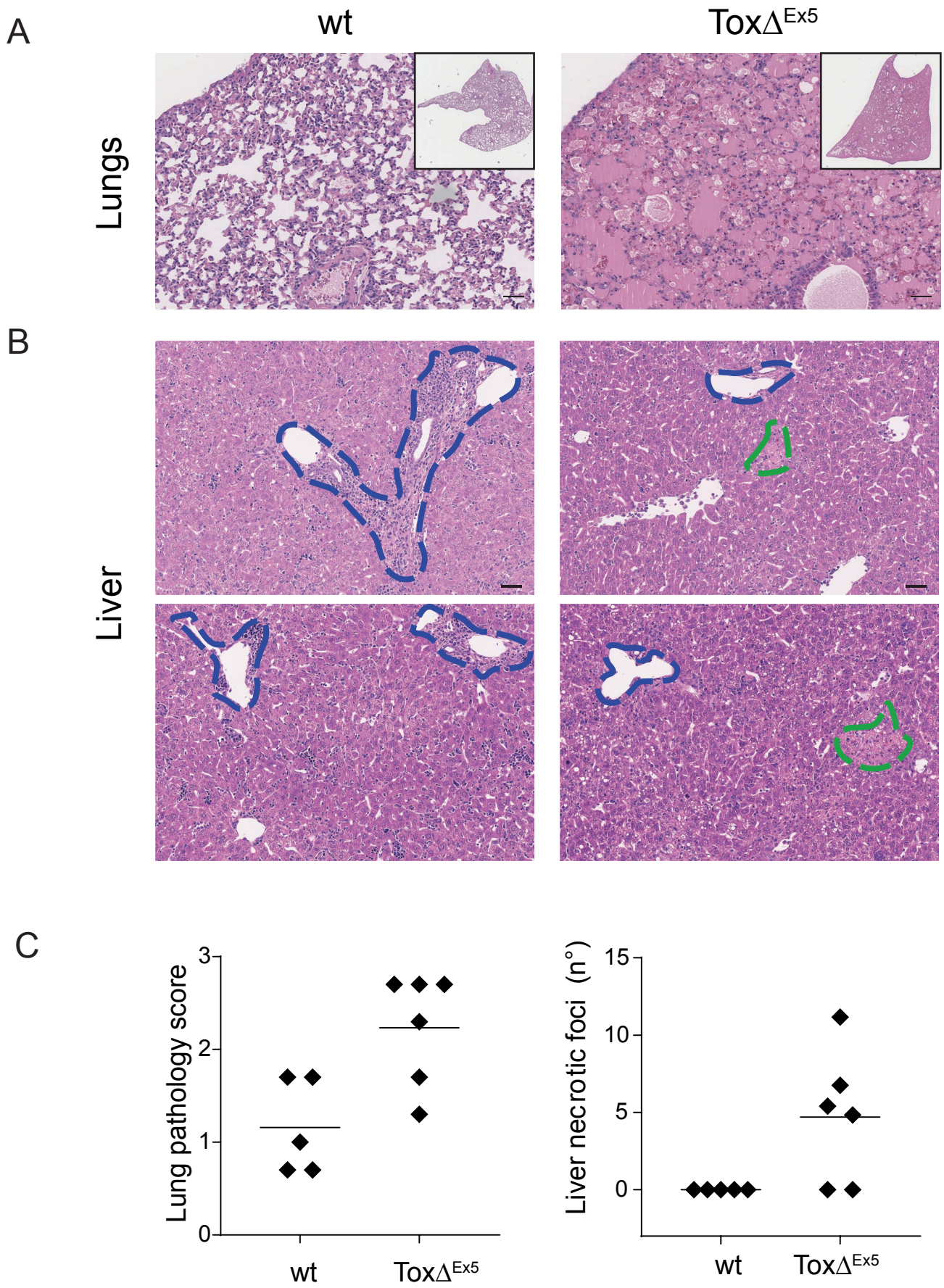

Supplementary Figure 11

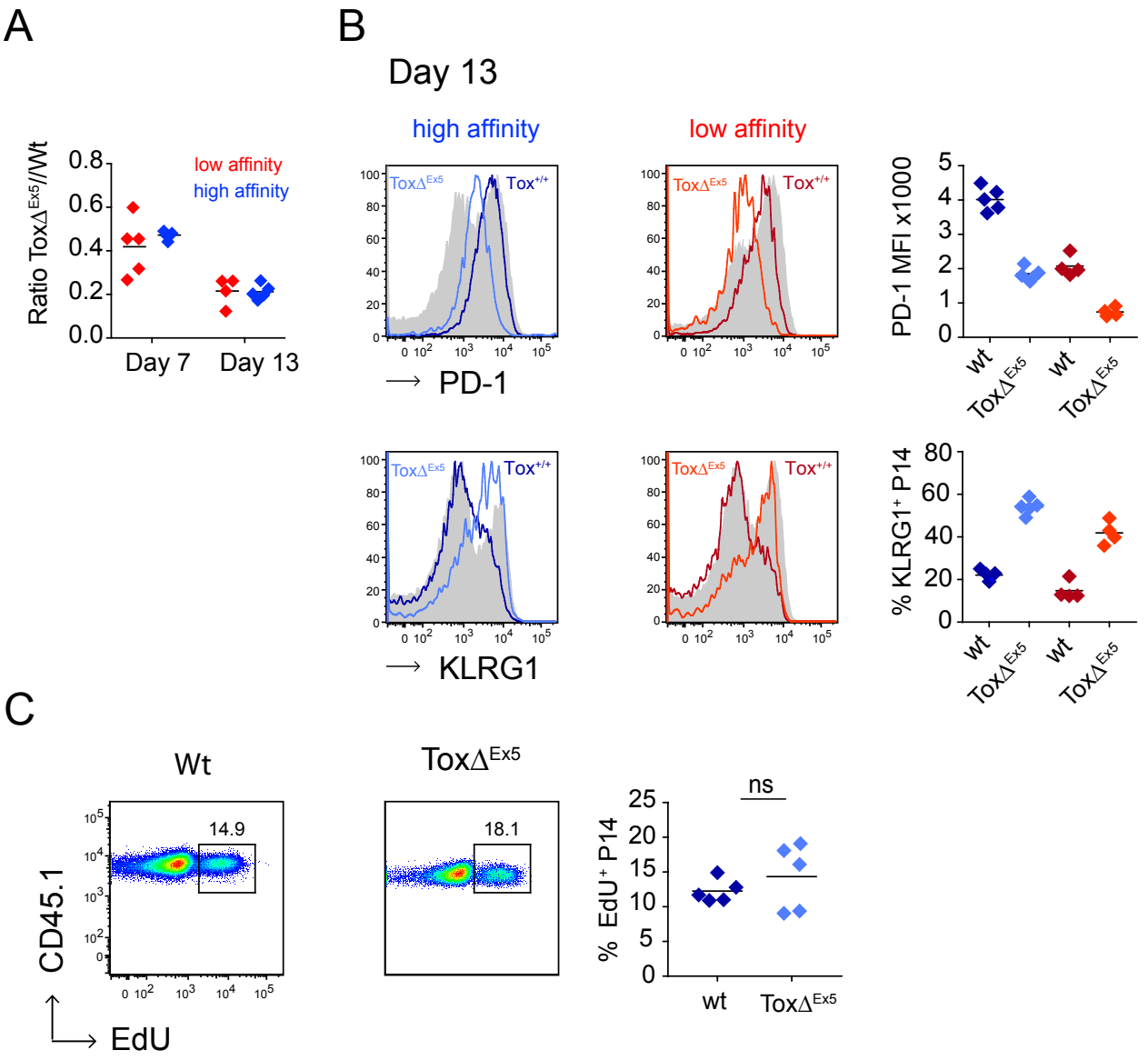

Supplementary Figure 12

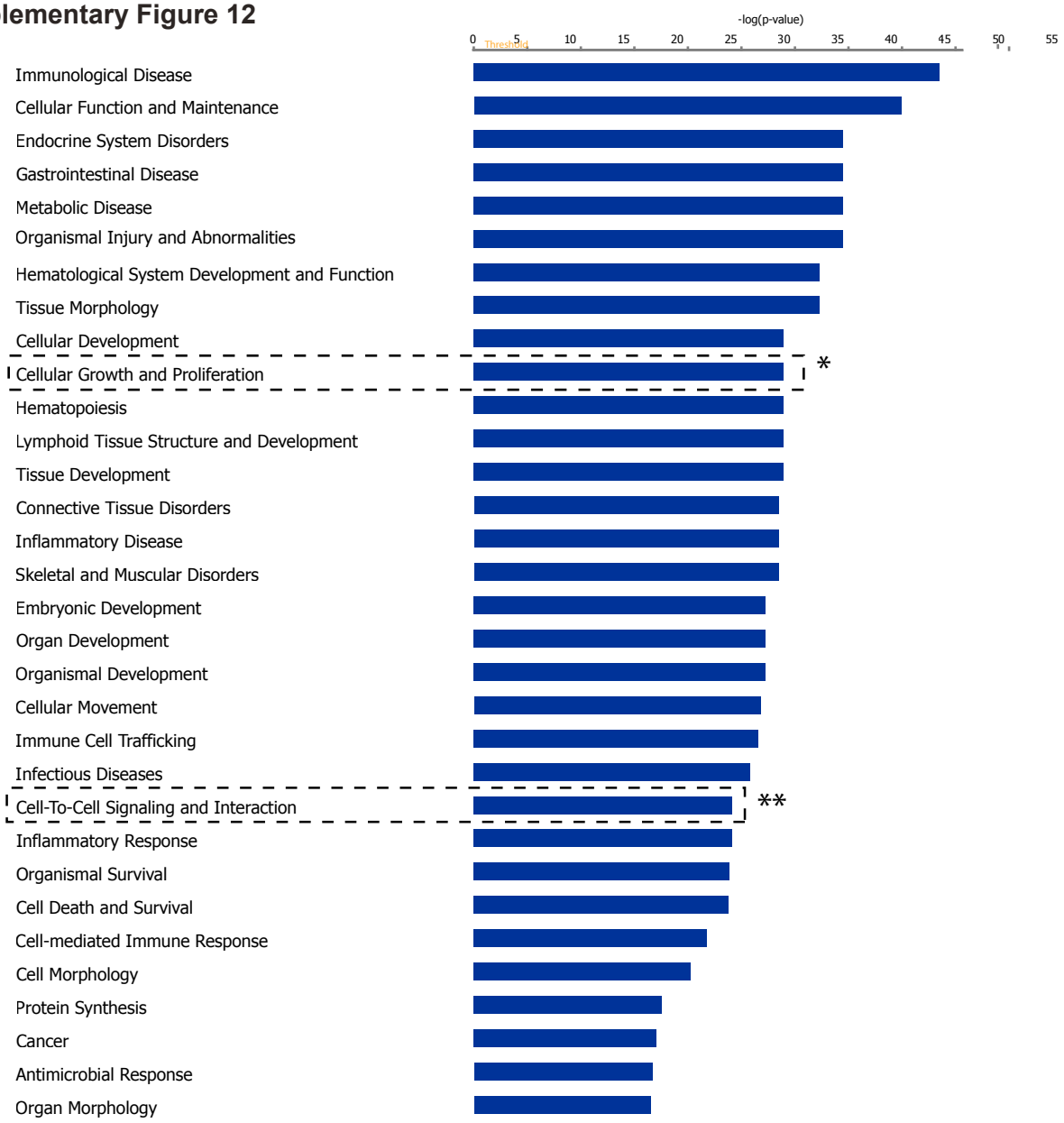

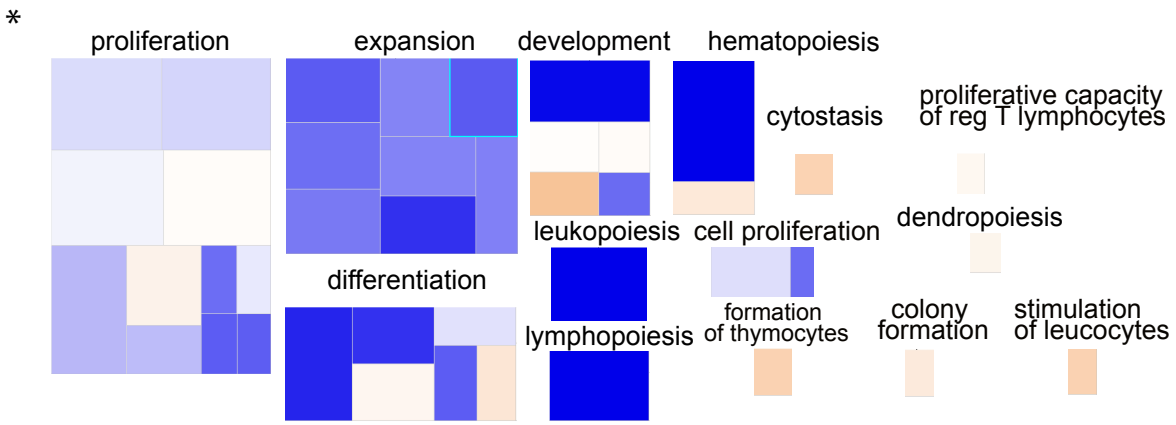

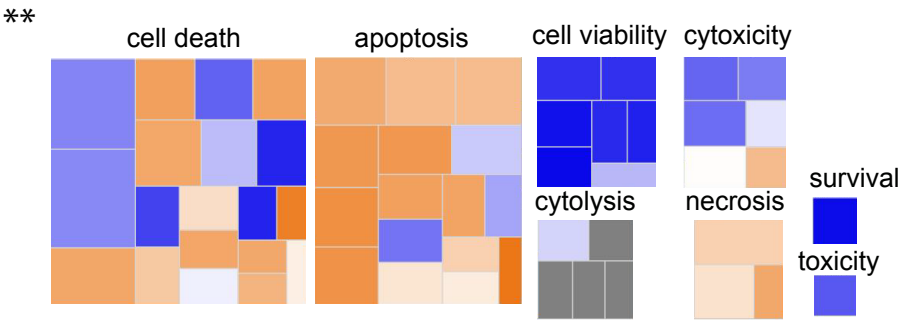

Supplementary Figure 13

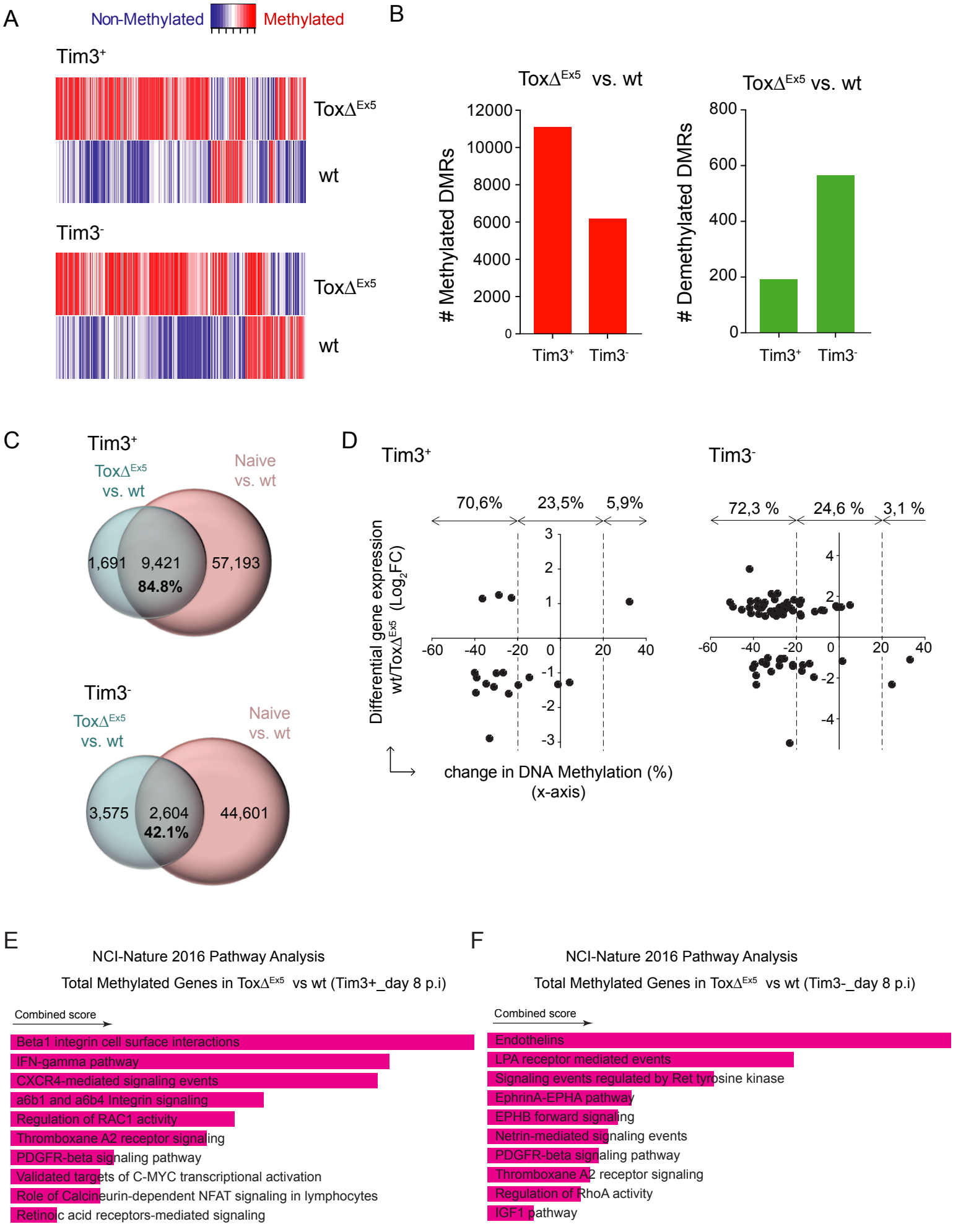

Supplementary Figure 14

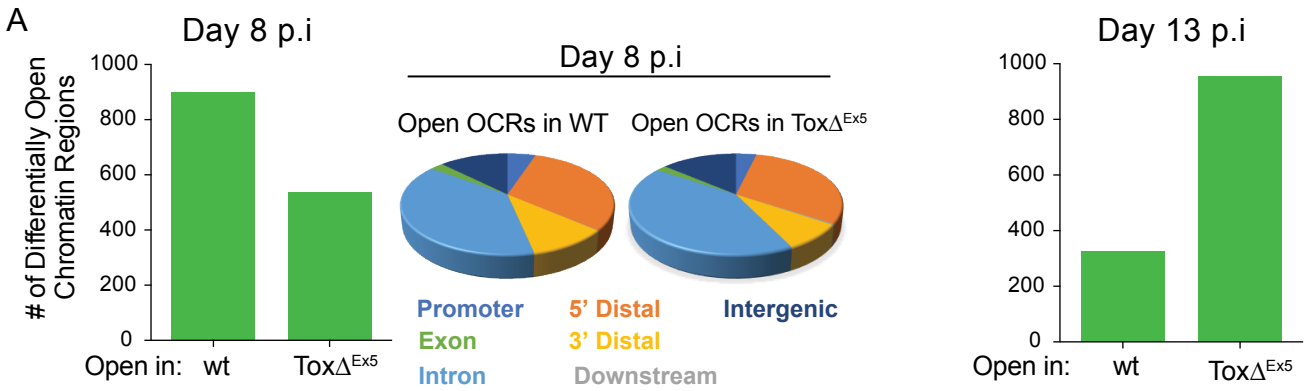

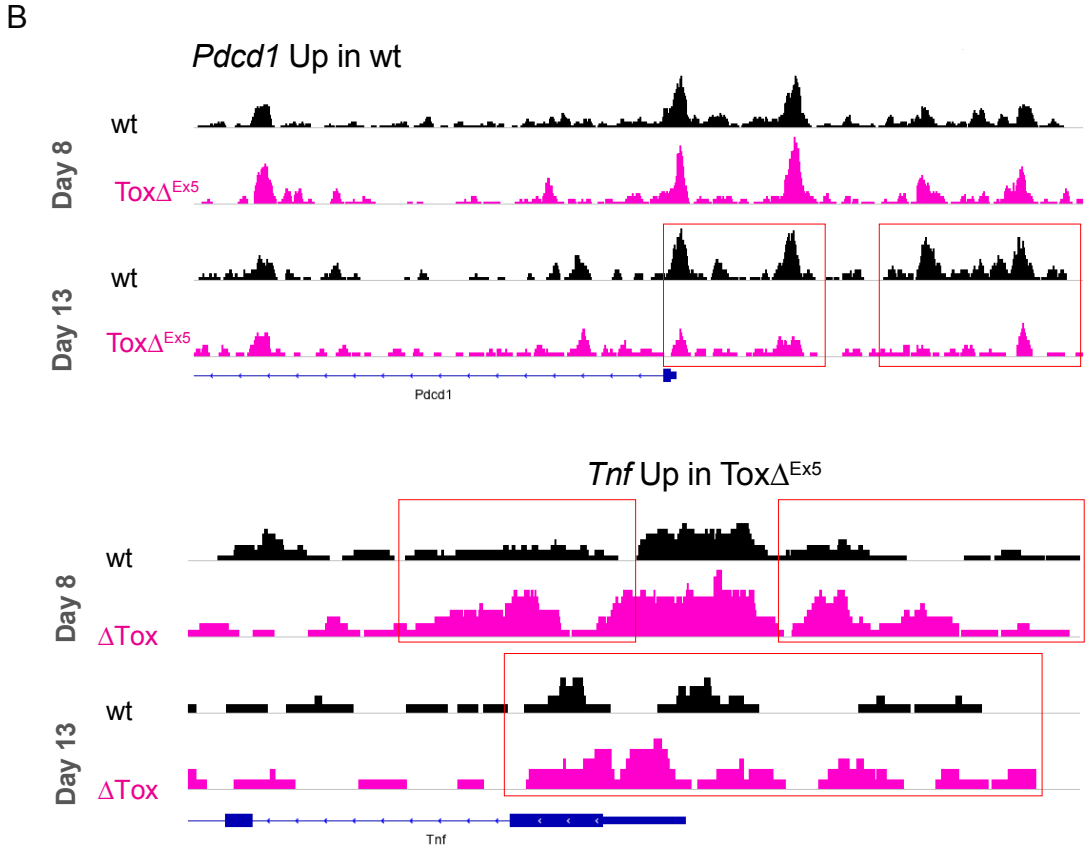

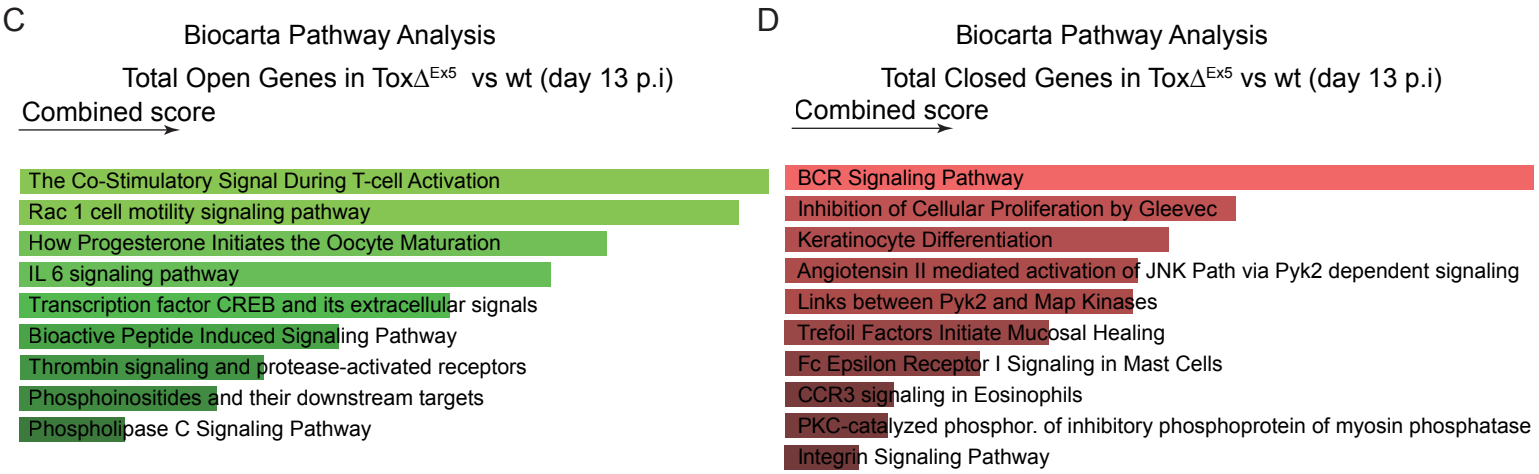

Supplementary Figure 15

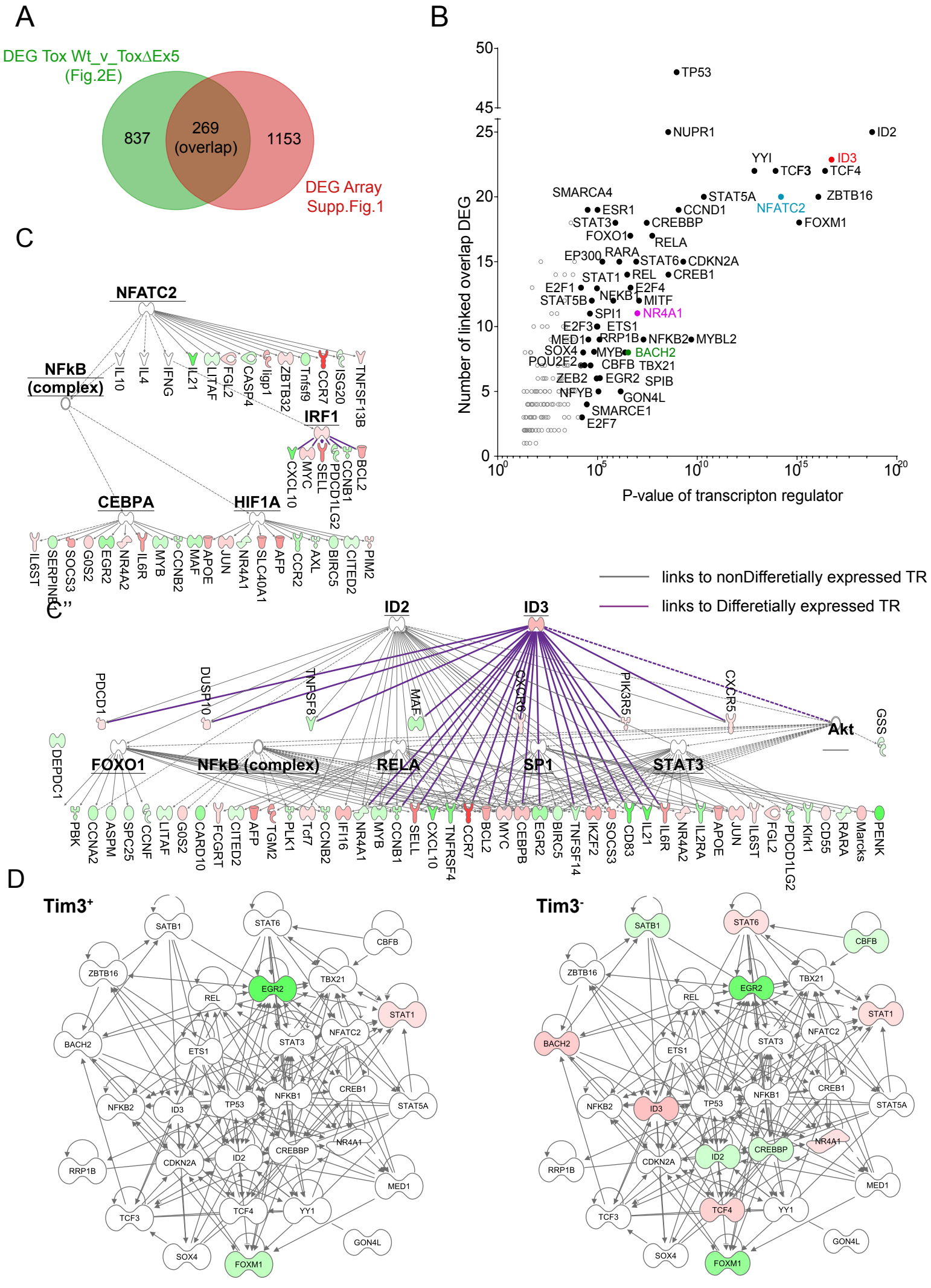

Supplementary Fig. 16